

1 **Geothermal heat flow in Antarctica: current and future**  
2 **directions**

3 Alex Burton-Johnson<sup>1</sup>, Ricarda Dziadek<sup>2</sup>, and Carlos Martin<sup>1</sup>

4 <sup>1</sup>British Antarctic Survey, High Cross, Madingley Road, Cambridge, CB3 0ET, UK

5 <sup>2</sup>Alfred Wegener Institute - Helmholtz Centre for Polar and Marine Research, Am Alten Hafen, Bremerhaven,  
6 Germany

7 *Correspondence to:* Alex Burton-Johnson (alerto@bas.ac.uk)

8 **1. Abstract**

9 Antarctic geothermal heat flow (GHF) affects the temperature of the ice sheet, determining its ability to slide and  
10 internally deform, as well as the behaviour of the continental crust. However, GHF remains poorly constrained,  
11 with few and sparse local, borehole-derived estimates, and large discrepancies in the magnitude and distribution  
12 of existing continent-scale estimates from geophysical models. We review the methods to estimate GHF,  
13 discussing the strengths and limitations of each approach, compile borehole and probe-derived estimates from  
14 measured temperature profiles, and recommend the following future directions: 1) Obtain more borehole-derived  
15 estimates from the subglacial bedrock and englacial temperature profiles. 2) Estimate GHF from inverse  
16 glaciological modelling, constrained by evidence for basal melting and englacial temperatures (e.g. using  
17 microwave emissivity). 3) Revise geophysically-derived GHF estimates using a combination of Curie depth,  
18 seismic, and thermal isostasy models. 4) Integrate in these geophysical approaches a more accurate model of the  
19 structure and distribution of heat production elements within the crust, and considering heterogeneities in the  
20 underlying mantle. And 5) continue international interdisciplinary communication and data access.

21

## 22 **1. Introduction**

23 The Antarctic ice sheet is the world's largest potential driver of sea level rise, and accurately modelling its  
24 dynamics relies, amongst others, on constraining conditions at the ice-bedrock interface. Measuring these basal  
25 conditions is inherently challenging and, of all the parameters affecting ice sheet dynamics, subglacial geothermal  
26 heat flow (GHF) is one of the least constrained (Larour et al., 2012; Llubes et al., 2006). Despite this uncertainty,  
27 GHF affects (1) ice temperature and, as a consequence, ice mechanical properties (rheology), (2) basal melting  
28 and sliding, and (3) the development of unconsolidated water-saturated sediments; all of which can promote ice  
29 flow (Greve and Hutter, 1995; Larour et al., 2012; Siegert, 2000; Winsborrow et al., 2010). Beyond ice dynamics,  
30 our knowledge of GHF allows us to model past and present basal melt rates in our exploration for old ice core  
31 climate records (Van Liefferinge et al., 2018), constrain models of glacial isostatic adjustment (GIA; van der Wal  
32 et al., 2013, 2015), and inform on the geological and tectonic development of Antarctica (McKenzie et al., 2005).

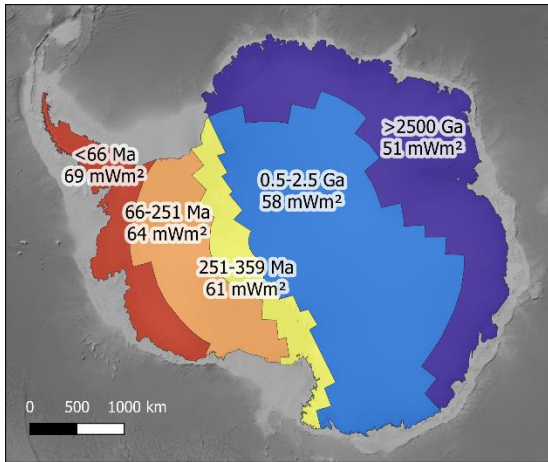
33 In recognition of the ambiguity and importance of Antarctic GHF, an increasing number of studies in geology,  
34 geophysics, and glaciology have sought to constrain this parameter, with a developing dedicated multinational  
35 interdisciplinary community (Burton-Johnson et al., 2019; Halpin and Reading, 2018). However, with an  
36 expanding research base and a requirement for multidisciplinary science, the necessity for a multidisciplinary  
37 review of current approaches and future directions was highlighted by the GHF sub-group of SERCE (Solid Earth  
38 Response and influence on Cryospheric Evolution) and the Scientific Committee on Antarctic Research (SCAR)  
39 (Burton-Johnson et al., 2019). This paper also provides the background material for a SCAR-commissioned White  
40 Paper on future research directions (Burton-Johnson et al., 2020).

### 41 **1.1. What is geothermal heat flow (GHF)?**

42 GHF describes the transport of heat energy from the interior of the Earth to the surface (Gutenberg, 1959; Pollack  
43 et al., 1993). This heat originates from two primary sources: 1) The primordial heat remaining from the formation  
44 of the Earth, when the kinetic energy of celestial collisions was transformed into heat energy; and 2) the  
45 radioactive decay of heat-producing elements (HPEs) and their isotopes; 98% of which is derived from Uranium,  
46 Thorium, and Potassium (Beardsmore and Cull, 2001; Lowrie, 2007). The HPEs are incompatible with the mineral  
47 structures of the mantle, so are concentrated into the crust (Boden, 2016; McDonough and Sun, 1995). Other  
48 sources of possible contributions to GHF are: 1) geoneutrino emission from the mantle (Huang et al., 2013;  
49 Korenaga, 2011), and 2) gravitational pressure (Elbeze, 2013; Morgan et al., 2016).

50 The estimated average heat flow of continental crust is  $67.1 \text{ mW m}^{-2}$ , whilst for oceanic crust it is  $78.8 \text{ mW m}^{-2}$   
51 (Lucazeau, 2019; although estimates vary according to sampling strategy and the number of observations). The  
52 difference between continental and oceanic heat flow reflects the smaller thickness of oceanic crust, with hot  
53 mantle rocks at comparatively shallow depths. Continental GHF varies significantly, primarily in response to  
54 variations in crustal heat production, age, composition, tectonic history, and thickness of crust and mantle  
55 (Mareschal and Jaupart, 2013). This results from the geological complexity of composite continental crust  
56 compared with oceanic crust. GHF is generally lower in stable crust away from convergent and divergent  
57 continental margins and rift basins, and higher in these magmatically active provinces (Lucazeau, 2019; Pollack  
58 et al., 1993). On a broad regional scale, continental GHF correlates negatively with age, allowing first order  
59 empirical estimation of Antarctic GHF based on its range of crustal ages (Fig. 1; Llubes et al., 2006; Sclater et al.,

60 1980). However, Antarctic crustal heat production estimates show high variability across sampled age ranges  
 61 (Gard et al., 2019), with lithology and tectonic setting being important controls on the heat production distribution  
 62 (Carson et al., 2014; Halpin et al., 2019).



63  
 64 **Fig. 1. Empirical estimation of GHF based on generalised Antarctic crustal ages and mean global GHF values of**  
 65 **continental crust of similar age (adapted from Llubes et al., 2006). Basemap bathymetry from ETOPO1 (Amante and**  
 66 **Eakins, 2009).**

67 The rate of heat flow,  $Q$ , can be approximated by the Fourier's Law (Baron Fourier, 1822). In the simple model  
 68 of a homogenous material with a constant thermal gradient, this equates to:

$$Q = -\kappa \partial T / \partial z$$

69  
 70 (1)

71 Where  $Q$  has the units  $\text{mW m}^{-2}$  (i.e. power per unit area);  $T$  is the temperature (K),  $z$  is the vertical distance (m);  
 72 and  $\kappa$  is the thermal conductivity of the material ( $\text{mW m}^{-1} \text{K}^{-1}$ ). When considering the basal conditions of the  
 73 Antarctic ice sheet, we are interested in the heat flow at bedrock surface. We also need to consider internal heat  
 74 production,  $A$  ( $\mu\text{W m}^{-3}$ ). For a simple case of constant thermal conductivity and heat production, surface heat flow  
 75 can be described by:

$$Q = \kappa_d [\partial T / \partial z]_d + \int A(z) \delta z$$

76  
 77 (2)

78 Where the integral is measured from the surface to a depth,  $d$  (equation 1.13 in Beardsmore and Cull, 2001).

79 We would like to highlight here that most methods to estimate GHF derive it from the temperature gradient, as in  
 80 Equations 1 and 2. However, these equations are a simplification, as temperature variation over time, surface  
 81 topography, internal heat production, and variation in the properties of the material all affect the observed  
 82 temperature gradient.

## 83 1.2. A note on terminology: Heat “Flow” vs Heat “Flux”

84 In the scientific literature, heat “flow” and heat “flux” are used interchangeably. The consensus from the SCAR-  
85 SERCE White Paper authorship (Burton-Johnson et al., 2020) is that “flow” is the correct terminology. “Heat  
86 flow” is not limited to the movement of material, but the mechanism of heat transfer (dominantly by conduction  
87 when near the Earth’s surface). Although the two terms are used interchangeably, heat “flow” has been established  
88 for decades to describe the rate of heat transferred across the surface of Earth per unit area, is the term used by the  
89 International Heat Flow Commission, and is thus the term used here. We recommend adopting this term in  
90 preference in the future, although the most important consideration is to state the correct units ( $\text{mW m}^{-2}$ ).

## 91 2. Motivation: What is the importance of GHF in Antarctica?

### 92 2.1. Glaciology

93 GHF can strongly influence the basal temperature of the ice sheet. As a consequence, it is a key contributor to  
94 basal meltwater production, ice rheology, basal friction, basal sliding velocity, and erosion (Fahnestock et al.,  
95 2001; Goelzer et al., 2017; Hughes, 2009).

96 The heat budget at the base of an ice sheet can be described (Vieli et al., 2018):

$$97 \quad Q_g + Q_s + Q_w + Q_p + Q_f + Q_c = 0$$

98 (3)

99 Where  $Q_g$  is the GHF,  $Q_s$  is the heat generated by sliding,  $Q_w$  is the heat generated by subglacial water flow,  $Q_p$   
100 is the heat required to maintain the flowing water at pressure melting point, and  $Q_f$  is the heat released by freezing  
101 or used by melting; and  $Q_c$  is the heat conducted away in the ice towards the ice surface. Of the positive  
102 contributions to basal heat, that generated by sliding ( $Q_s$ ) can be orders of magnitude greater than that from GHF  
103 ( $Q_g$ ), but in slow flowing areas  $Q_s$  is negligible and GHF plays a key role in the heat budget (Larour et al., 2012;  
104 Pittard et al., 2016a).

105 To illustrate this point, Llubes et al. (2006) modelled a  $20 \text{ mW m}^{-2}$  increase in GHF across the Antarctic continent  
106 (from uniform values of  $40$  to  $60 \text{ mW m}^{-2}$ ). This resulted in a  $6^\circ\text{C}$  increase in the mean basal temperature, from -  
107  $13^\circ\text{C}$  to  $-7^\circ\text{C}$ , and expanded the proportion of the basal ice area above the pressure melting point (PMP) from  
108  $16\%$  to more than  $50\%$ . This variation directly affects the basal melt rates, with a uniform  $40 \text{ mW m}^{-2}$  generating  
109  $6.7 \text{ km}^3 \text{ yr}^{-1}$  of basal melting across Antarctica, whilst  $60 \text{ mW m}^{-2}$  would generate  $18 \text{ km}^3 \text{ yr}^{-1}$ . However, unlike  
110 the GHF values used, the resultant basal temperature variation is non-uniform: Although the two heat flow models  
111 produce only a few  $^\circ\text{C}$  difference in basal temperature near the coast, they generate up to  $15^\circ\text{C}$  difference in  
112 central East Antarctica. This is because horizontal advection and frictional basal heating are negligible beneath  
113 the thick, slow moving ice of East Antarctica, and surface temperatures have a reduced effect on basal conditions  
114 (Llubes et al., 2006; Pollard et al., 2005). In these regions of thick ice, the increased pressure brings the basal ice  
115 temperature closer to its PMP (Pollard et al., 2005), and the thicker ice has a greater insulating effect. Although  
116 the effect of pressure of basal temperature is much smaller than surface temperature variation, in areas where of  
117 thick ice where the basal temperature is close to the PMP, even small variation in GHF can determine whether

118 basal melting occurs. This has a resultant effect on the basal friction and sliding of the ice sheet (Pollard et al.,  
119 2005). In addition, the increased ice temperature makes it more susceptible to internal deformation, which also  
120 enhances its ability to flow (Llubes et al., 2006).

121 Even beneath the comparatively thinner ice of West Antarctica, the sensitivity of basal temperature to heat flow  
122 is enhanced (Llubes et al., 2006). There is evidence that this region, dominated tectonically by the West Antarctic  
123 Rift System (Jordan et al., 2020), exhibits very high values of basal heat flow and resultant basal melting  
124 (Schroeder et al., 2014). Above  $85 \text{ mW m}^{-2}$ , the basal temperature of much of the West Antarctic Ice Sheet will  
125 pass its pressure melting point (in agreement with radar evidence for extensive basal melting; Llubes et al., 2006;  
126 Rémy and Legresy, 2004; Schroeder et al., 2014). Consequently, enhanced basal heat flow in West Antarctica can  
127 have a large effect on its basal melt rates, although the thinner ice sheet in West Antarctica compared to East  
128 Antarctica makes it more sensitive to surface parameters (advection and conduction of the surface temperature,  
129 itself influenced by the accumulation rate; Llubes et al., 2006).

130 In addition to enhancing basal melting and reducing basal friction, increased GHF enhances ice flow by increasing  
131 the englacial temperature and thus reducing the ice stiffness (Larour et al., 2012). Because the heat produced by  
132 basal friction and viscous deformation can be orders of magnitude greater than from GHF in fast-flowing ice  
133 streams, this effect is only significant in upstream, slow-flowing areas (Larour et al., 2012). In these regions of  
134 thick, slow-flowing ice, even local high heat flow anomalies of insufficient heat for basal melting can result in the  
135 development of accelerated, channelised flow for hundreds of kilometres upstream and downstream of the GHF  
136 anomaly through the effect of GHF on the ice rheology (Pittard et al., 2016a). Regions along ice divides and  
137 adjacent to ice streams are particularly sensitive to enhanced GHF (Pittard et al., 2016b).

138 Whilst the points above highlight the necessity of estimating Antarctic GHF, it is very important that the accuracy  
139 of these estimates can be verified. The impact of inaccurate GHF constraints on models of ice sheet dynamics  
140 have been shown by comparing GHF estimates for Greenland. Ice sheet modelling controlled by spatially variable  
141 GHF forcing reproduces the observed state to only a limited degree, and fails to reproduce either the topography  
142 or the low basal temperatures measured in southern Greenland (Rogozhina et al., 2012). Instead, an unrealistic  
143 spatially uniform GHF forcing produces a considerably better fit. If the much larger Antarctic ice sheet is to be  
144 accurately modelled, the accuracy of the GHF estimates used must be well constrained by multiple independent  
145 methodologies, sensitivity tests, and comparison of different models.

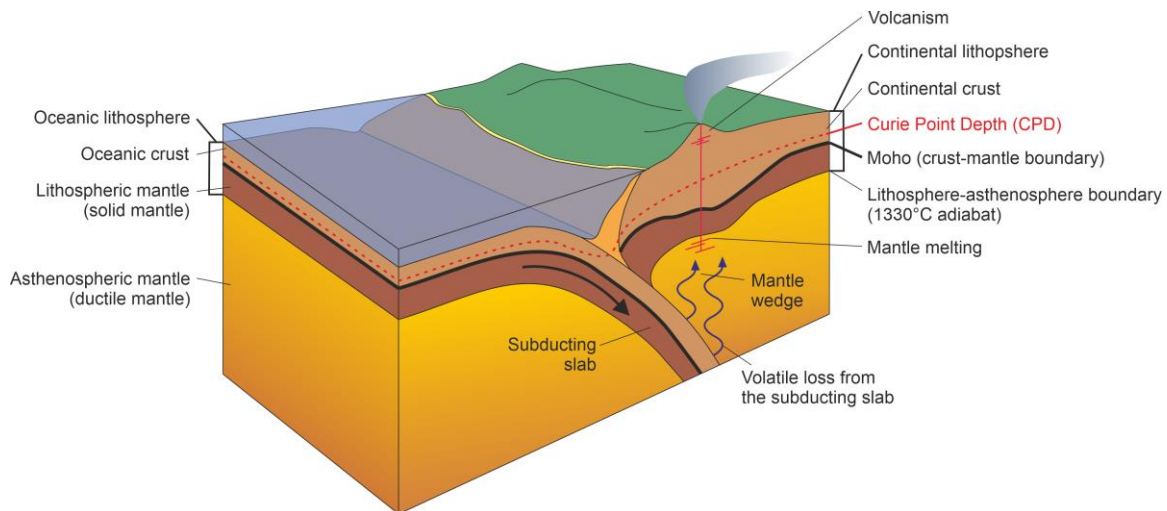
146 Recently, there has been increasing interest in the exploration of suitable locations for coring Antarctica's oldest  
147 continuous ice record (Fischer et al., 2013). This problem requires accurate knowledge of GHF, as basal melt rates  
148 limit the maximum possible age of recoverable ice (Van Liefferinge et al., 2018). Additionally, due to  
149 environmental concerns around possible drilling fluid contamination, frozen bed conditions are a prerequisite for  
150 deep coring operations for recovery of the oldest ice records.

## 151 2.2. Glacial Isostatic Adjustment (GIA)

152 The temperature of the lithosphere and upper mantle are important parameters for modelling the isostatic response  
153 to changes in the volume of the overlying ice sheet (i.e. glacial isostatic adjustment, GIA). This is because the  
154 (visco-)elastic properties of the lithosphere and mantle directly relate to its thermal properties (Chen et al., 2018;

155 Kuchar and Milne, 2015). GIA is a critical component of the long-term evolution of ice sheets and could  
156 potentially stabilise retreating ice streams in submarine settings (Barletta et al., 2018; Kingslake et al., 2018). Of  
157 particular importance here is that the temperature-dependant viscosity that controls GIA can be modelled using  
158 surface heat flow estimates (van der Wal et al., 2013, 2015).

## 159 2.3. Geology and tectonics



160

161 **Fig. 2. Basic illustration of a subduction zone at a convergent margin between oceanic and continental lithosphere to**  
162 **clarify the geological concepts and terms used in this paper.**

### 163 2.3.1. Mantle dynamics

164 Heat flow variation and its isostatic effects (i.e. the buoyancy control on crustal elevation, resulting from the  
165 different densities of the dense mantle and less dense overlying crust) provide evidence for mantle dynamics  
166 beneath a continent. For example, high heat flow anomalies have been proposed as evidence for sub-lithospheric  
167 heating by present and past mantle plumes (regional hot spots of warm mantle upwelling beneath the lithosphere;  
168 e.g. Courtney and White, 1986; Martos et al., 2018), and the absence of enhanced heat flow where mantle ascent  
169 is proposed has been used to argue against such processes (e.g. Stein and Stein, 2003). Also, because of the  
170 relationship between surface heat flow and isostatic elevation, heat flow studies can reveal thermal or  
171 compositional variation of the sub-continental mantle, as a reduction in its density can increase the isostatic  
172 elevation of the surface topography (Hasterok and Gard, 2016).

### 173 2.3.2. Development of the lithosphere

174 The thermal properties of the lithosphere control its response to tectonic deformation (e.g. Sandiford and Hand,  
175 1998), such as the development of crustal shear zones and earthquakes. The lithosphere's thermal properties also  
176 affect the relative density of lithosphere and underlying mantle, and (as a result of this buoyancy effect) the  
177 isostatic surface elevation. This in turn influences the heights of Antarctica's mountain ranges and the depths of  
178 its sedimentary basins (McKenzie et al., 2005). For these reasons, understanding the continent's GHF will inform  
179 on the development of many of Antarctica's largest tectonic features. For example, the lithospheric extension of

180 the West Antarctic Rift System, the prominent elevation of the Transantarctic Mountains, the deep topographic  
181 depression of the Wilkes subglacial basin, and the extensive Palmer Land Shear Zone of the Antarctic Peninsula.  
182

Section	Method	Description	Advantages	Disadvantages
<b>3. Measured Temperature Gradients</b>				
3.1.	Bedrock boreholes	GHF estimated from measured temperature gradient into bedrock boreholes.	- Local estimates of GHF derived directly from the bedrock.	- Only point estimates. - Affected by local variation. - Requires drilling through the ice sheet and deep enough into the rock.
3.2.	Ice boreholes	Temperature gradient measured in ice boreholes, and GHF estimated from the basal temperature gradient or models of the temperature profile.	- Provides local estimates of GHF beneath the ice sheet without drilling into bedrock.	- The ice sheet must be frozen to the bed and thermally equilibrated. - Limited by modelling accuracy of the ice sheet thermal history - Hot water drilling requires 2 years for thermal equilibration after drilling.
3.3.	Marine/onshore sediment temperature probes	GHF estimated from shallow (<10m) temperature gradient measured using gravity-driven probes.	- Faster acquisition than borehole estimates, as no drilling required.	- Requires deep water without long-period temperature variation.
<b>4. Geophysical and geological methods</b>				
4.1.	Magnetic-derived estimates	Temperature gradient calculated by estimating the depth of the Curie isotherm from magnetic anomalies.	- Allows continent-scale estimates. - Does not require models of the crust and mantle structure.	- Assumes that the depth to the bottom of the magnetic source is temperature controlled (i.e. it represents the Curie isotherm), despite possible other geological controls. - Spatial resolution limited by altitude of sensor and depth of magnetic source.
4.2.	Seismic-derived estimates	Calculate GHF empirically or via forward modelling using the relationship of mantle seismic velocity and temperature, and estimation of lithospheric thickness.	- Allows continent-scale estimates. - Empirical models utilise well-constrained regions. - Forward models estimate the geological source of GHF.	- Empirical estimates assume global comparison is valid. - Forward models assume mantle and crustal composition. - Limited spatial resolution.
4.3.	Gravity model-derived estimates	Calculates GHF from models of crust and mantle structure derived from gravity estimates of crustal thickness.	- Allows large-scale GHF estimates. - Incorporates constraints on crustal composition.	- Models are non-unique, requiring further constraints. - Assumes values of crustal and mantle composition.
4.4.	Conjugate margin-derived estimates	Reconstruct the Gondwana supercontinent, interpolating Antarctic GHF from better constrained adjacent continents.	- Utilises regions where GHF is better constrained. - Should be most accurate around continental margins.	- Poor constraints away from continental margins. - Affected by choice of input data and interpolation method.
4.5.	Isostatic elevation	Calculates GHF from topography using a compositional correction.	- The topographical input is a well constrained variable.	- Requires assumptions of crustal thickness, density, heat production, and thermophysical properties. - Low spatial resolution.
4.6.	Incorporating heterogeneous crustal compositions.	Incorporating measurements of crustal heat production and models of heterogeneous crustal structure into geophysical GHF models.	- A more realistic representation of the geological sources of GHF. - Reflects the concentration of heat production in the crust.	- Requires assumptions of the subglacial geology away from outcrops. - The 3D structure and composition of the crust and mantle is ambiguous.
<b>5. Glaciological methods</b>				
5.1.	Subglacial water	Radar evidence for subglacial water used to model the required GHF distribution for required basal melting and hydrology.	- Based on observable effects of GHF.	- Requires accurate ice sheet thermal models. - Subglacial water only accumulates in appropriate topographic depressions.
5.2.	Subglacial lakes	Lakes identified by enhanced radar reflectivity, and the minimum GHF required for basal melting estimated from ice sheet thermal models.	- Based on observable effects of GHF. - Where the ice sheet is frozen to the bed, maximum GHF can be calculated.	- Requires accurate ice sheet thermal models. - Subglacial water only accumulates in appropriate topographic depressions.
5.3.	Englacial stratigraphy	Melt rates and required GHF calculated from englacial layers identified in radar data.	- Based on observable effects of GHF. - Identifies high GHF anomalies.	- Requires accurate data and interpolation from ice cores. - Requires accurate ice sheet thermal models.
5.4.	Microwave emissivity	Englacial temperatures modelled with variable GHF to simulate observed satellite-derived, temperature dependent microwave radiation.	- Derives more extensive englacial temperature profiles than can be achieved by boreholes.	- Only applicable to areas of thick, slow flowing ice. - Method requires further validation.

**Table 1. Summary of methods to estimate GHF and their section in the manuscript.**

184 **3. GHF estimates from measured temperature gradients**

185 Having highlighted the importance of constraining Antarctica's GHF, the following sections discuss current  
186 approaches to its estimation. The methods discussed are summarised in Table 1.

187 Local heat flow estimates can be derived by measuring the temperature at various depths below the surface (either  
188 in the bedrock, overlying sediments, or within the ice sheet) and deriving a temperature gradient. In Antarctica,  
189 GHF has been derived through temperature measurements from boreholes into the bedrock or into the ice sheet,  
190 and also from probes into unconsolidated sediments. It is important to recognise that these are "estimates" not  
191 "measurements" of GHF, particularly when using them to verify the accuracy of geophysical or inverse GHF  
192 estimates. This is because the measured thermal gradient can be affected by processes other than GHF, including  
193 surface temperature variation and hydrothermal circulation. When evaluating a specific local estimate, its  
194 derivation, local geology, and other regional GHF estimates must be considered. Thermal gradients and surface  
195 heat flow may vary significantly over 10 km lateral spatial resolutions (Carson et al., 2014) with variations in  
196 geology (affecting heat production and conductivity; Carson et al., 2014; Hasterok and Chapman, 2011),  
197 hydrothermal circulation (affecting local heat convection and redistribution; Fisher and Harris, 2010), and  
198 topography (affecting heat diffusion pathways to the surface; Bullard, 1938; Lees, 1910).

199 **3.1. Boreholes into bedrock**

200 The thermal gradient can be determined by measuring the temperature variation at different depths in the crust.  
201 Away from Antarctica, these measurements are from boreholes (commonly those drilled for mineral or  
202 hydrocarbon exploration), mineshafts, caves, or other cavities. The temperature gradient of the crust's uppermost  
203 10-50 m is dominantly affected by downward conduction of the surface temperature rather than GHF. To address  
204 this, temperature measurements are made over the largest depth range possible (typically 100-1000 m).

205 Borehole temperature measurements are made using wire-line temperature probes, with a thermistor at the leading  
206 tip and measurements made progressively downwards to minimise disturbance of the borehole fluids prior to  
207 temperature measurement. The temperature is measured from the bore fluid, not the surrounding rock, so an  
208 important consideration is the need for thermal equilibration of the wall rock and the borehole fluids following  
209 drilling and prior to measurement. In addition, the heat produced during drilling needs to be dissipated from the  
210 borehole. As a guide, 10-20 times the drilling time is required before a borehole is equilibrated to within  
211 instrument accuracy (Bullard, 1947; Jaeger, 1956), although observations show that after 3 times the drilling time,  
212 borehole fluids are within 0.05°C of equilibrium values (Lachenbruch and Brewer, 1959). As an example of the  
213 time required for bedrock drilling, drilling of the multiple Cape Roberts Project boreholes averaged 16-31 m day<sup>-1</sup>  
214 (Talalay and Pyne, 2017). For the low water flows used in small-core (<4 cm diameter) diamond drilling  
215 (compared with the high water flows of wider core diameter rotary drilling), heat exchange is negligible except  
216 for the upper and lowermost ~20 % of the borehole, and full temperature profile measurements can be taken about  
217 two days after drilling cessation (Jaeger, 1961, 1965).

218 Depth below the bedrock surface must be considered when taking borehole temperature measurements. Where  
219 terrestrial bedrock is exposed, atmospheric temperature and seasonal variation perturbs the thermal gradient in the  
220 upper >100 m of the crust. In Antarctica, temperatures from Hole 3 of the Dry Valley Drilling Project provided  
221 estimates of "equilibrium" gradient only when deeper than 90 m (Decker, 1974; Decker et al., 1975; Pruss et al.,

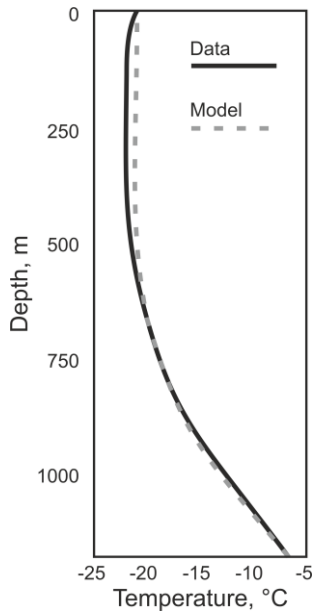
222 1974). It may be possible to compensate for seasonal variation in shallower boreholes using long-term  
223 observations of the temperature gradient (>1 year), although the previous attempt (from a 7.6 m borehole at  
224 McMurdo Station; Risk and Hochstein, 1974) derived an anomalously high GHF estimate ( $164 \text{ mW m}^{-2}$ , compared  
225 to  $66 \text{ mW m}^{-2}$  from a 260 m deep borehole; Decker and Bucher, 1982).

226 Subglacial bedrock is not exposed to atmospheric temperature variation, so the geothermal gradient can be  
227 measured from shallower depths. However, it is affected by heat derived from the overlying ice sheet: internal  
228 and basal frictional shear heating from the ice sheet, heat advection, basal water, and seasonal temperature  
229 variation (e.g. Ritz, 1987). In the absence of a deep, borehole-derived, subglacial bedrock temperature profile, the  
230 depth required to accurately measure the unperturbed geothermal temperature gradient is currently unknown.  
231 Thermal diffusion modelling over timescales of low frequency climate variation may constrain this.

### 232 3.2. Ice boreholes

233 Subglacial GHF can be estimated from the temperature gradient from boreholes into the ice sheet (e.g. Engelhardt,  
234 2004; Fudge et al., 2019; Nicholls and Paren, 1993). This requires that there is no additional heating from basal  
235 shear or horizontal advection, and that the ice sheet has been unequivocally frozen to the bed for long enough that  
236 the bedrock and overlying ice sheet have thermally equilibrated. To meet this requirement, the temperature profile  
237 is best measured from cores into the summits of ice domes where the ice sheet is stationary (Engelhardt, 2004).  
238 As applies to bedrock boreholes, a delay between drilling and temperature measurement is required for the thermal  
239 disturbance from the drilling to dissipate. For hot-water drilling, this can take 2 years (Barrett et al., 2009;  
240 Engelhardt, 2004). The temperature profile is typically measured using thermistors, recording the temperature  
241 through changes in resistivity to electrical currents. Either a string of thermistors is deployed into the borehole  
242 prior to freezing, and the temperature recorded over time, or the hole can be kept open with drill fluid and  
243 downhole temperature measured with a moving thermistor. More recently, temperature has been recorded also  
244 using distributed temperature systems (DTS; Suárez et al., 2011; Ukil et al., 2011). The temperature is derived  
245 from the travel time of a laser beam within an optical fibre. All of these methods require thermal equilibration.

246 Once the englacial temperature profile is obtained, GHF estimation can be achieved through three methods.  
247 Firstly, if the borehole reaches the ice-bedrock interface, and the bedrock and overlying ice are in thermal  
248 equilibrium, then the GHF can be estimated in the same way as for bedrock boreholes (e.g. Engelhardt, 2004).  
249 That is, using the temperature gradient in the ice near the ice-bedrock interface but using the thermal conductivity  
250 of ice rather than rock (Equation 1). Secondly, rather than measuring a temperature profile above the bed, the  
251 basal temperature at the ice-bedrock interface can be measured, and temperature modelled through time to  
252 constrain the required GHF (e.g. Fudge et al., 2019). Thirdly, if the borehole doesn't reach bedrock, and similarly  
253 to the previous method, a thermal model is required to constrain GHF (e.g. Zagorodnov et al., 2012). In the  
254 methods where modelling is required, the variables are modified within constraints determined for the location  
255 until the modelled temperature profile best fits the measurements (Fig. 3), and the modelled temperature gradient  
256 within the bedrock used for GHF calculation.



257

258 **Fig. 3. An example of temperature measurements (solid black line) and steady state model (dashed grey line) from**  
 259 **which GHF can be estimated. Adapted from (Dahl-Jensen et al., 1999) for Law Dome ice borehole temperature profile.**  
 260 **Note that it is the deeper temperature gradient that is modelled rather than the shallower temperature variation.**

261 In regions where the ice sheet is frozen to the bed and thermally equilibrated, GHF can be estimated from  
 262 boreholes that do not reach the bedrock providing that the temperature profile is obtained below the penetration  
 263 depth (or skin depth,  $\delta$ ) of surface temperature variation into the ice sheet. This depth is defined by the circular  
 264 frequency of the variation ( $\omega$ ), and the thermal diffusivity of the material ( $k$ ) according to Equation 4 (Fig. 4;  
 265 Carslaw and Jaeger, 1959; Wangen, 2010).

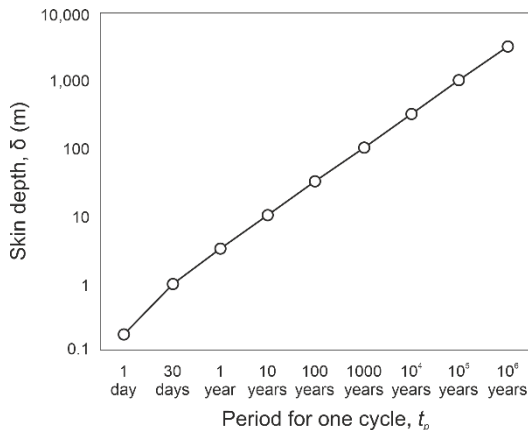
$$266 \quad \delta = \sqrt{(2k/\omega)}$$

267 (4)

268 Where circular frequency ( $\omega$ ) is defined by Equation 5, where  $t_p$  is the time for one period (or cycle) of the  
 269 temperature variation (Wangen, 2010).

$$270 \quad \omega = 2\pi/t_p$$

271 (5)



272

273 **Fig. 4. Relationship between skin depth and periodicity of temperature variation through a material of thermal**  
274 **diffusivity,  $k$ , of  $10^{-6} \text{ m}^2 \text{ s}^{-1}$ . This diffusivity is comparable to ice at  $-10^\circ\text{C}$  (James, 1968), or average values of a range**  
275 **of rock types at  $-50^\circ\text{C}$  (Vosteen and Schellschmidt, 2003), and increases with decreasing temperature for both**  
276 **materials.**

277 The deepest significant perturbations of the englacial temperature profile are from glacial-interglacial cycles, and  
278 GHF is best estimated from the englacial temperature profile below the depth at which this effect becomes  
279 negligible. In Greenland, this is the bottom 20 % of the ice sheet, but in areas of low-accumulation in Antarctica  
280 this can extend to much shallower depths. With sufficiently accurate temperature measurements, the full  
281 temperature profile of the ice sheet and the subglacial GHF may be estimated from boreholes penetrating only the  
282 upper 600 m or 20 % of the total ice sheet thickness (Hindmarsh and Ritz, 2012; Mulvaney et al., 2019; Rix et al.,  
283 2019). However, use of shallow boreholes to estimate GHF use simplified thermal models and assumptions on  
284 ice sheet evolution, and so require further validation.

285 However, poorly-constrained thermal effects within the ice sheet propagate uncertainties in GHF estimates from  
286 ice sheet boreholes (Cuffey and Paterson, 2010, Chapter 9). This is a particular problem if there is any ambiguity  
287 as to whether the ice sheet is frozen to the bed. The englacial temperature profile depends on heat sources at the  
288 surface, base, and within the ice (i.e. internal deformation-derived frictional heating). Heat sources that act at the  
289 base of the ice, such as frictional heating by basal motion, are impossible to differentiate from GHF.

### 290 3.3. Marine and onshore unconsolidated sediments

291 Shallow ( $< \sim 10$  m) temperature gradients in unconsolidated sediments can be recorded using gravity-driven probes  
292 rather than drilled boreholes. They carry multiple thermistors along the length of the probe that provide a  
293 temperature profile. These measurements can be taken from unconsolidated sediments offshore (e.g. Dziadek et  
294 al., 2019, 2017), in subglacial lakes (Fisher et al., 2015) or below ice shelves (Begeman et al., 2017).

295 As applies to borehole measurements, temperature gradients in unconsolidated sediments must be taken at  
296 sufficient depth to represent the crustal temperature gradient and not be perturbed by temperature variation in the  
297 overlying water or ice (i.e. they must be representative of steady-state conditions). The penetration depth of  
298 temperature variation is dependent on its frequency (Equation 4 and Fig. 4; Carslaw and Jaeger, 1959).  
299 Consequently, diurnal or annual cycles only affect the upper few centimetres to couple of metres of the surface  
300 temperature profile, whilst variations over the last 200-300 years will affect the upper 200 m, and post-glacial  
301 warming can be observed down to 2500 m. These effects are dampened by an overlying water column or ice sheet,  
302 but temperature variation over 10 kyr can still affect basal ice sheet temperatures (Engelhardt, 2004). Although  
303 large ( $>10^\circ\text{C}$ ) seasonal temperature variations are dampened by  $\sim 90\%$  at water depths of 3-5 m (Müller et al.,  
304 2016), long-term variations (e.g. climate-controlled variations in Circumpolar Deep Water over the last  $\sim 12$  kyr;  
305 Hillenbrand et al., 2017) are likely recorded in the upper 3 m at 400 m water depth, 2 m at 700 m depth, and even  
306 the upper  $\sim 1$  m at 1000 m depth (Dziadek et al., 2019).

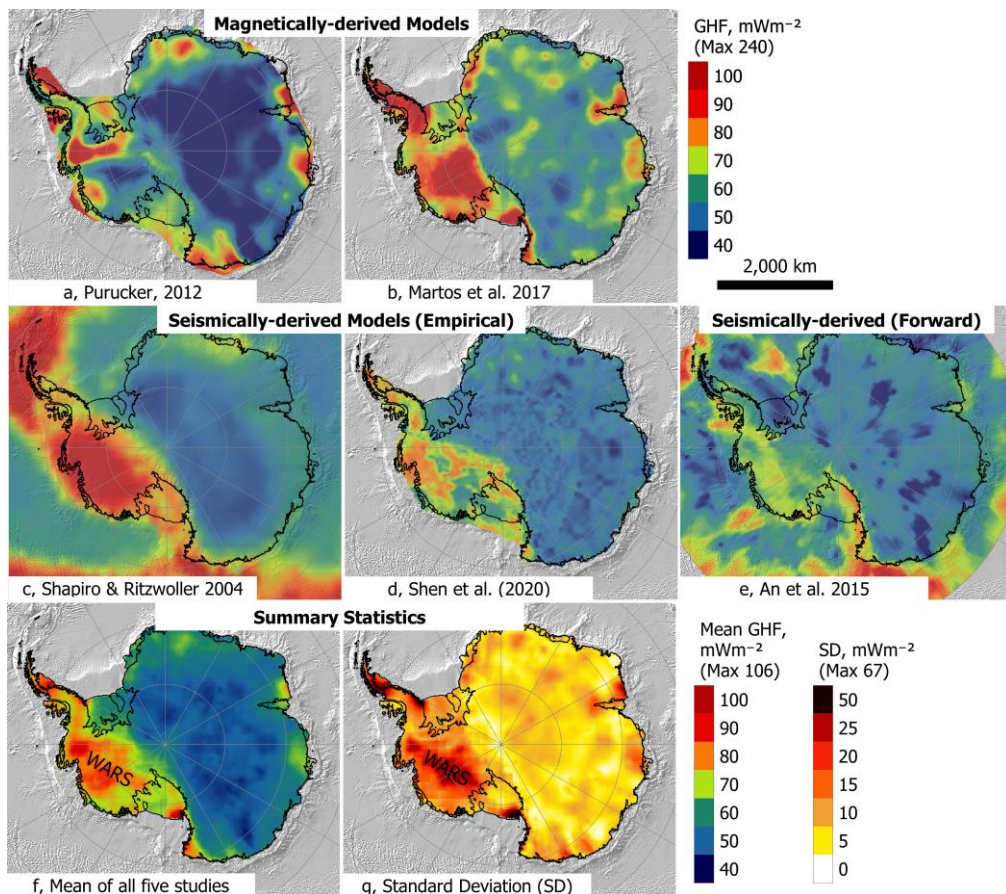
307 Similarly to borehole temperature measurements, a time delay must be considered between penetration of the  
308 sediments and temperature measurement. A ten minute delay between sediment penetration and measurement is

309 sufficient to allow decay of frictional heating, as the temperature decay takes  $\sim 100$  s (Dziadek et al., 2019; Pfender  
 310 and Villinger, 2002).

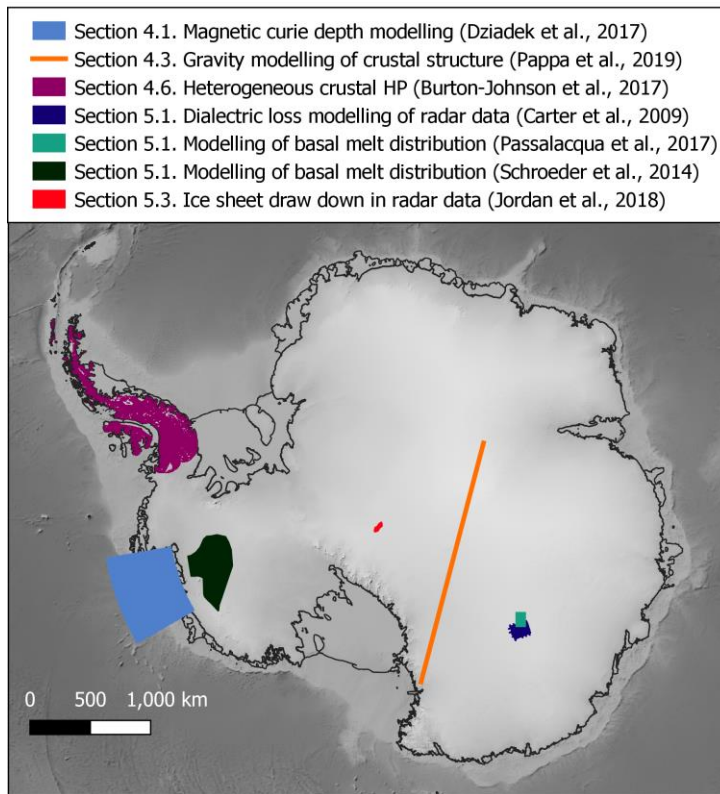
311 Unconsolidated temperature measurements can also be taken from marine boreholes (e.g. IODP boreholes). For  
 312 bedrock boreholes, a delay is required between drilling and measurement for thermal equilibration of the wall  
 313 rock and the borehole fluids, which would be problematic for marine boreholes where a drill ship cannot remain  
 314 on site. Instead, for boreholes into unconsolidated sediments, a probe is deployed into the borehole bottom  
 315 sediments shortly after drilling. Although technology has improved (Davis et al., 1997; Heesemann et al., 2006),  
 316 measurements can be affected by frictional heating during and after probe deployment, or by movement of water  
 317 and sediments within the hole. Only measurements that exhibit the expected temperature decay rate after  
 318 penetration are thus reliable (Hyndman et al., 1987).

#### 319 4. Geophysical and geological methods to estimate GHF

320 In addition to the few and sparse penetrative GHF estimates in Antarctica, continental (Fig. 5) and regional (Fig.  
 321 6) estimates have been derived from both solid Earth (geophysical/geological), and glaciological data and models.



322  
 323 **Fig. 5. Continent-scale geophysical estimates of GHF derived from magnetic Curie depth estimates (a and b; Martos et**  
 324 **al., 2017, and Purucker, 2012 - an update of Fox Maule et al, 2005) and seismic models (c to e; An et al., 2015b; Shapiro**  
 325 **and Ritzwoller, 2004; Shen et al., 2020). The mean and standard deviation of the combined studies are given in f and**  
 326 **g, (available in the Supplementary Material), highlighting the large disparities in West Antarctica. WARS – West**  
 327 **Antarctic Rift System.**



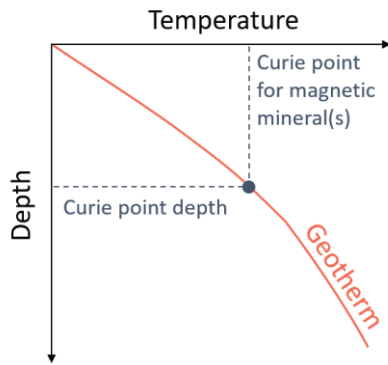
328

329 **Fig. 6. Coverage of sub-continental scale regional estimates of GHF, with reference to the section where the data is**  
 330 **discussed.**

331 **4.1. Magnetic-derived estimates**

332 As for the penetrative methods of GHF estimation described above (Section 3), geophysical methods also derive  
 333 GHF from a temperature gradient. In this case, magnetic survey data is used to determine the depth at which the  
 334 maximum temperature of ferromagnetic magnetisation is exceeded (the Curie temperature; Haggerty, 1978). This  
 335 Curie temperature is different for different minerals, but is assumed in these studies to be the Curie temperature  
 336 of magnetite (580 °C) as this mineral is most commonly the dominant contributor to crustal magnetisation (Bansal  
 337 et al., 2011; Fox Maule et al., 2005; Langel and Hinze, 1998).

338 Above the Curie temperature, rocks lose their ability to maintain ferromagnetic magnetisation (e.g. Haggerty,  
 339 1978). The depth of this isotherm in the crust (the Curie Point Depth, CPD; Fig. 7 and Fig. 2) is thus assumed to  
 340 be the depth to the bottom of the magnetic source (DBMS) determined from magnetic survey data. The DBMS  
 341 maps a transition zone, rather than an exact depth (Haggerty, 1978), and can provide information on crustal  
 342 temperatures at depths not accessible by other means (Andrés et al., 2018; Okubo et al., 1985). Regions found to  
 343 have a shallower DBMS (and thus an assumed shallower CPD) are expected to have higher average temperature  
 344 gradients, and, therefore, higher GHF (e.g. Aboud et al., 2011; Andrés et al., 2018; Arnaiz-Rodríguez and  
 345 Orihuela, 2013; Bansal et al., 2013, 2011; Bhattacharyya and Leu, 1975; Guimarães et al., 2013; Li et al., 2017;  
 346 Obande et al., 2014; Okubo et al., 1985; Ross et al., 2006; Salem et al., 2014; Tanaka et al., 1999; Trifonova et  
 347 al., 2009).



348

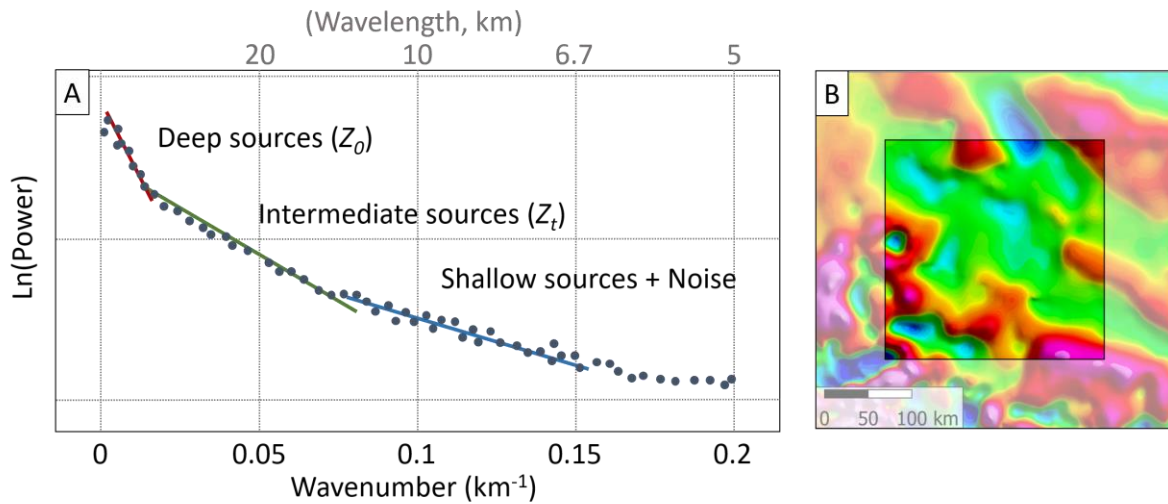
349 **Fig. 7. Approximation of the geothermal gradient from the Curie point depth (CPD). The CPD is assumed to mark the**  
 350 **base of the magnetic crust (DBMS).**

351 The first Antarctic-wide magnetically-derived GHF map (Fox Maule et al., 2005; updated by Purucker, 2012, Fig.  
 352 5a) used the “equivalent source magnetic dipole method” (Mayhew, 1979) to map magnetic anomalies from  
 353 multiple satellites at different altitudes as evenly distributed magnetic dipoles on the Earth’s surface (Dyment and  
 354 Arkani-Hamed, 1998). Due to filtering of the data during processing, this magnetic anomaly distribution is only  
 355 susceptible to shallow, short-wavelength magnetic variation. To calculate the CPD, a long-wavelength CPD model  
 356 was modified until it reproduced the determined short-wavelength anomalies. The temperature gradient  
 357 represented by this CPD was combined with assumed homogenous crustal properties (heat production and  
 358 conductivity) to model the surface heat flow. Due to the high altitude of the satellite data, the horizontal resolution  
 359 of this approach was limited to at least a few hundred kilometres.

360 Spectral methods are the alternative and more commonly applied approach to estimating the DBMS, analysing  
 361 the spectrum of wavelengths in magnetic profiles or gridded data (e.g. Blakely, 1996; Okubo et al., 1985; Spector  
 362 and Grant, 1970). These methods depend on the implicit assumption that long wavelength features result from  
 363 deep sources. The depth of this source is calculated from a “power spectrum” (Fig. 8) of wavenumber (the inverse  
 364 of the wavelength) against the logarithm of each wavenumber’s “power” (the square of each wavelength’s  
 365 magnitude after conversion by a Fast Fourier Transformation to describe the spectrum of wavelengths in the  
 366 signal). From this power spectrum (Fig. 8) the top ( $Z_t$ ) and centre ( $Z_0$ ) of the deepest magnetic layer are inferred  
 367 from the slope of the intermediate and long wavelength zone of the spectra derived from magnetic anomaly data.  
 368 The DBMS ( $Z_{DBMS}$ ) stems from the simple geometric relationship between these depths:

369 
$$Z_{DBMS} = 2Z_0 - Z_t$$

370 (6)



371

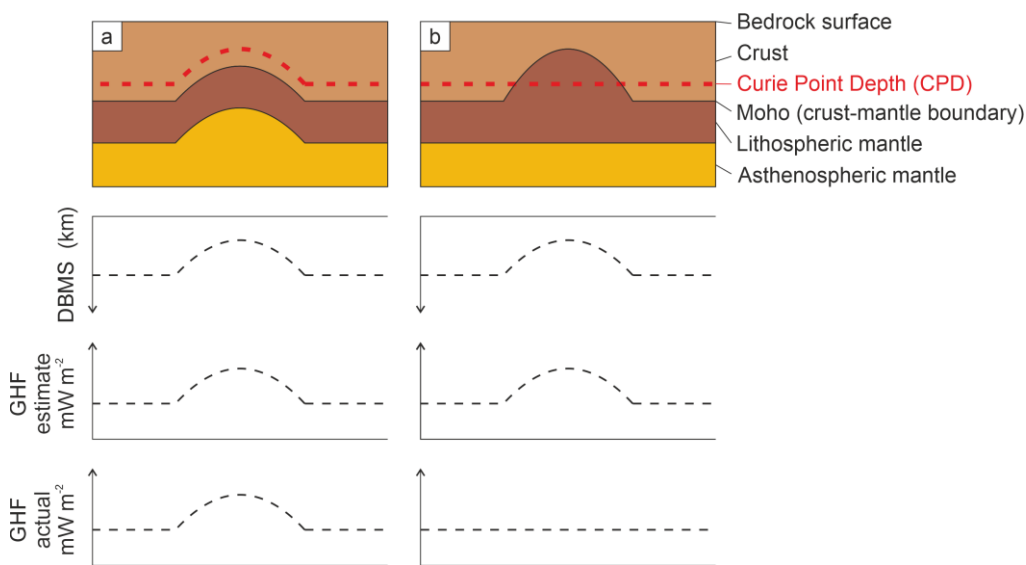
372 **Fig. 8. A) Identification of the slopes of the intermediate and long wavelength magnetic anomalies from the power**  
 373 **spectrum of magnetic anomalies within a single magnetic window (B). For illustration, small circular anomalies in the**  
 374 **magnetic window (B) would correspond to shallow sources in the power spectrum, whilst larger anomalies would**  
 375 **correspond to intermediate and deep sources.**

376 To map the DBMS across a study area, the spectra of magnetic anomalies are computed within overlapping  
 377 rectangular windows regularly spaced over the aeromagnetic map. Particularly for gridded data, the dimensions  
 378 of the region chosen to analyse the long wavelength frequencies must be sufficiently large to capture the DBMS.  
 379 Ravat et al. (2007) elaborate that the dimension of the region analysed may need to be (in some cases) up to 10  
 380 times the DBMS, but that dimensions exceeding 200 to 300 km may average different large-scale crustal  
 381 structures. This suggests that satellite data, which typically detects magnetic anomalies in that wavelength, may  
 382 not be suitable for this spectral method of CPD estimation. Choosing the window size therefore forces a trade-off  
 383 between accurately determining the DBMS within each sub-region and resolving small changes in DBMS between  
 384 sub-regions (Ross et al., 2006).

385 Spectral methods have been applied in Antarctica (Dziadek et al., 2017; Martos et al., 2017a; Purucker and  
 386 Whaler, 2007; Fig. 5b and Fig. 6) to combined satellite and airborne magnetic anomaly data (e.g. ADMAP;  
 387 Golynsky et al., 2006; Maus, 2010). The results show a general agreement at a continental scale, but vary  
 388 significantly on a regional scale (Fig. 5). This is related to the resolution of the magnetic anomaly data, particularly  
 389 in regions where only satellite magnetic data are available. Furthermore, regional-scale magnetic anomaly  
 390 databases are usually a mosaic of individual aeromagnetic surveys. Ross et al. (2006) emphasise that subtle  
 391 discontinuities along survey boundaries are caused by differences in survey specifications, such as flight line  
 392 spacing, flight altitude, regional field removal, or the quality of data acquisition. These, for instance, may  
 393 contaminate the long-wavelength signal caused by deep magnetic sources (Grauch, 1993). Long wavelength  
 394 features can also result from shallow but spatially extensive sources, such as volcanic provinces, and can lead to  
 395 an underestimation of the DBMS.

396 CPD estimates assume a homogenous magnetic mineralogy of magnetite, and thus a Curie temperature of 580 °C  
 397 (Bansal et al., 2011; Fox Maule et al., 2005; Langel and Hinze, 1998). This assumption neglects the compositional  
 398 variability in plutonic rocks that lead to Curie temperature ranges between 300 °C and 680 °C, and in cases of

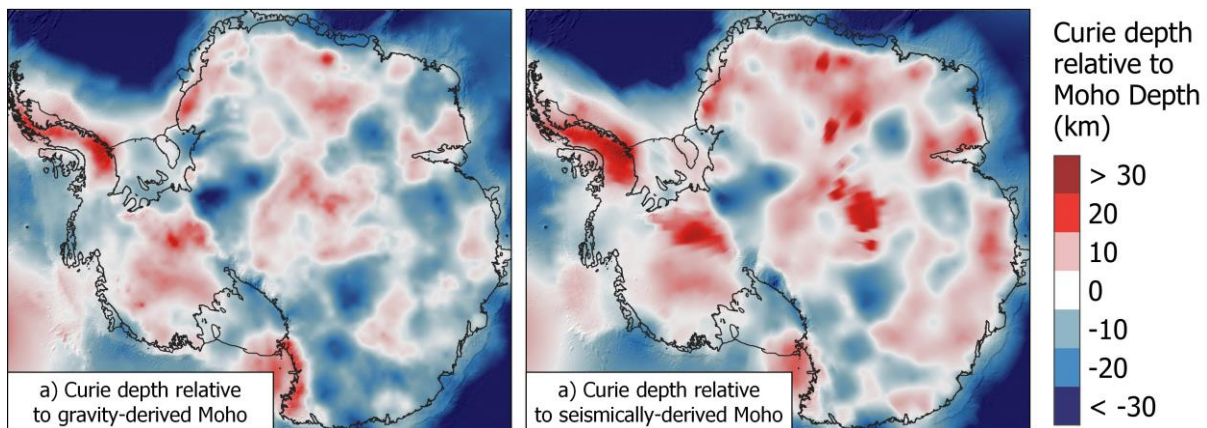
399 magnetic assemblages of Fe-Ni-Co-Cu metal alloys up to 620 °C to 1084 °C (Haggerty, 1978). Without further  
 400 constraints and validations, these assumptions remain the best approach, especially in sparsely sampled regions  
 401 like Antarctica, but introduce uncertainties of several kilometres in Curie depths and consequent uncertainties in  
 402 GHF estimates (Bansal et al., 2011; Ravat et al., 2007). Similarly, in areas of thin crust, non-magnetic mantle  
 403 rocks can be shallower than the Curie depth. In these regions, the calculated CPD will appear shallower due to a  
 404 lack of magnetic minerals in the mantle rocks (Fig. 9.; Frost and Shive, 1986; Wasilewski and Mayhew, 1992).  
 405 This can be investigated through comparison of the Antarctic Curie depth estimates with the seismically- or  
 406 gravitationally-derived depth of the crust-mantle boundary (the Moho depth; Fig. 10 and Fig. 2). For example,  
 407 thermal modelling of seismic, gravity, and magnetic data showed the DBMS of the Norwegian margin reflected  
 408 the basement geometry, not the CPD, and that surface heat flow estimates using magnetic CPD models were thus  
 409 unreasonably high (Ebbing et al., 2009).



410

411 **Fig. 9. Two scenarios illustrating the ambiguity in estimating Curie point depth (CPD) and GHF. a) Estimates from a**  
 412 **region with a shallow CPD over an area of thin crust. b) Similar but incorrectly interpreted estimates from a region of**  
 413 **shallow non-magnetic mantle rocks. In scenario (b), the DBMS is shallower despite there being no deviation in the CPD**  
 414 **depth. DBMS: Depth to the bottom of the magnetic source (assumed to represent the CPD in the GHF estimates**  
 415 **discussed).**

416



417 **Fig. 10. Comparison of Curie depth (Martos et al., 2017) and depth of the crust-mantle boundary (the Moho depth)**  
418 **derived from a) gravity modelling (Pappa et al., 2019b), and b) seismic modelling (An et al., 2015a). Negative values**  
419 **show areas where the estimated Curie depth is deeper than the estimated Moho depth, and positive values are where**  
420 **the Curie depth is shallower than the Moho depth.**

421 However, whilst in general the Earth's mantle does not contribute to the magnetic signal (due to its weak  
422 magnetisation and high temperature conditions), in some cases the Curie depth may indeed lie within the mantle.  
423 This occurs where metallic magnetic phases in the mantle beneath old, tectonically stable crust ("cratons"; Ferré  
424 et al., 2013) or subduction regions (e.g. Blakely et al., 2005) contribute to mantle magnetisation. In these settings  
425 the crust-mantle boundary should not be considered an absolute magnetic boundary (Ferré et al., 2013). This  
426 implies that if in a given region the Moho depths are shallower than the deepest magnetic layer, a magnetic mantle  
427 at temperatures below the Curie temperature may be considered. However, even in these cases the upper mantle  
428 susceptibility will be more than 1-2 magnitudes smaller than the overlying crust. This is not considered in current  
429 spectral methods assuming constant susceptibility. Consequently, Curie depth methods yield non-unique  
430 solutions, and further available constraints and observations need to be considered, when interpreting the Curie  
431 temperature distribution (e.g. geological evidence, borehole measurements, and Moho depth estimates).

#### 432 4.2. Seismic-derived estimates

433 Temperature is the dominant control on seismic velocity in the mantle (e.g. Carlson et al., 2005), and hence the  
434 mantle heat flow at the base of the Antarctic crust can be determined from seismic data. By determining the change  
435 in seismic velocities marking the density discontinuity at the lithosphere-asthenosphere boundary (Fig. 2) the  
436 depth of the 1330°C isotherm can be estimated. This is the "mantle adiabat" marking the top of the seismic low-  
437 velocity zone, and the change from a solid to ductile mantle (Fig. 2). The continental-scale GHF can then be  
438 estimated by assuming the heat production and conductivity of the lithosphere above this boundary, and  
439 integrating this with the seismically-derived mantle heat flow (An et al., 2015b; Fig. 5d). However, the  
440 seismically-derived, continent-scale Antarctic GHF model of An et al. (2015a) (Fig. 5d) is limited to a lateral  
441 spatial resolution of >120 km, assumes a laterally uniform crustal structure, and is insensitive to the lithospheric  
442 geotherm (instead it inversely correlates with crustal thickness).

443 Composition also affects seismic velocities. For example, a 2% increase in velocity can be explained either by a  
444 120°C decrease in temperature, a 7.5% depletion in iron, or a 15% depletion in aluminium (Godey et al., 2004).  
445 Slow mantle velocities at subduction zones can also be caused by water or hydrous fluids serpentinising the mantle  
446 wedge (Fig. 2; Kawakatsu and Watada, 2007). However, velocity in the Antarctic seismic model (An et al., 2015b)  
447 does not account for variability of mantle compositions, mineralogy, grain size, or water content of the mantle or  
448 crust. An uncertainty in the lithospheric thickness of 15-30 km was assumed by (An et al., 2015b) based on the  
449 150°C temperature uncertainty, but ~50 km uncertainty for ~200 km thick lithosphere may be more accurate  
450 (Artemieva, 2011; Godey et al., 2004). In addition, seismological models suffer from limited and inconsistent  
451 spatial coverage, which can lead to discrepancies in upper mantle velocities and differences in Moho depths (Fig.  
452 2) up to 10 km, even for the same receiving station (An et al., 2015b supporting information; Pappa et al., 2019).

453 Some constraints on the mantle and lithosphere composition can be determined from xenoliths (rock fragments  
454 of the deep crust or mantle entrained in magma rising from depth) or exposed deep crustal sections, where

455 variation in temperature and composition with depth can be determined from the metamorphic minerals present.  
456 Constraints can also be derived empirically by comparing the seismic velocity with similar regions. Shapiro and  
457 Ritzwoller (2004) (Fig. 5c) extrapolated global heat flow measurements to Antarctica based on the assumption  
458 that structurally similar regions have similar magnitudes of GHF. This was achieved by calculating a spatially  
459 variable “similarity functional” determined from the differences between the seismic velocity and seismic Moho  
460 depth between a location of interest and a comparable location elsewhere. A histogram of heat flow measurements  
461 could then be assigned to the location of interest in Antarctica based on the similarity-weighted sum of  
462 measurements from structurally similar regions, and the mean values of these distributions mapped as continental  
463 heat flow. Spatial resolution was limited to the lateral resolution of the global shear velocity model across  
464 Antarctica (600-1000 km; Shapiro and Ritzwoller, 2002). Although the studies of Shapiro and Ritzwoller (2004)  
465 and An et al. (2015a) both used seismic data and are thus frequently compared, it is important to highlight that  
466 they use very different approaches in deriving heat flow (the former employing a probabilistic approach and the  
467 latter using forward modelling).

468 The empirical seismically-derived model for Antarctica has recently been revised (Fig. 5d; Shen et al., 2020).  
469 Rather than the low-resolution global database used by Shapiro and Ritzwoller (2004), an Antarctic seismic model  
470 was derived and compared with the high-resolution seismic model and GHF measurements of the USA; again  
471 calculating spatially variable similarity functionals to compare the data. Recognising the non-unique solutions  
472 provided by this method, Shen et al. (2020) also map the associated uncertainties of their model.

#### 473 4.3. Gravity model-derived estimates

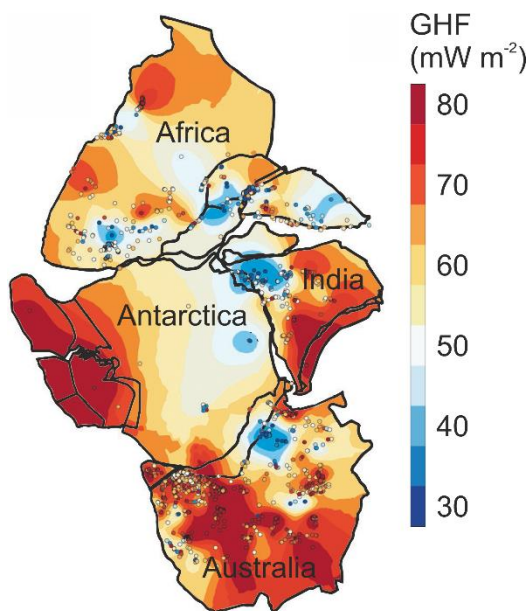
474 Satellite gravity data has been used as an alternative to seismic modelling to determine crustal thickness. Pappa  
475 et al. (2019b) used satellite gravity data, a model of global gravity variation (the “geoid”), surface and bedrock  
476 topography, and assumed rock and ice densities to calculate the topographically-corrected variation of gravity in  
477 Antarctica (the “Bouguer anomaly”), from which the depth of the crust-mantle boundary could be calculated. This  
478 approach to calculate crustal thickness is sensitive to long-wavelength (>150 km) features representing deep  
479 structures, rather than short-wavelength, near surface density changes. However, gravity-modelling solutions are  
480 non-unique, and require additional constraints on the density contrast between the crust and mantle at a reference  
481 depth, and/or seismic depth constraints on crustal thickness.

482 Using the gravity-derived crustal thickness estimates, cross-sectional models of the mantle and lithospheric  
483 structure were calculated, with adjustments made to crustal density and crustal thickness until the models reflected  
484 the observed variation in gravity and elevation (Pappa et al., 2019b). By assigning assumed values of heat  
485 productivity and thermal conductivity values to the modelled cross-sections, surface heat flow was calculated  
486 along the line of the modelled cross-section (Fig. 6).

#### 487 4.4. Conjugate margin-derived estimates

488 An alternative approach to constrain the probable GHF of East Antarctica is to compare it with its Gondwanan  
489 conjugate margins, reconstructed prior to the breakup of the supercontinent (Fig. 11). Plate tectonic  
490 reconstructions indicate that the subglacial geology of East Antarctica is comparable to the margins of Australia,  
491 Africa, and India (Aitken et al., 2016; Daczko et al., 2018; Ferraccioli et al., 2011; Flowerdew et al., 2013; Mulder

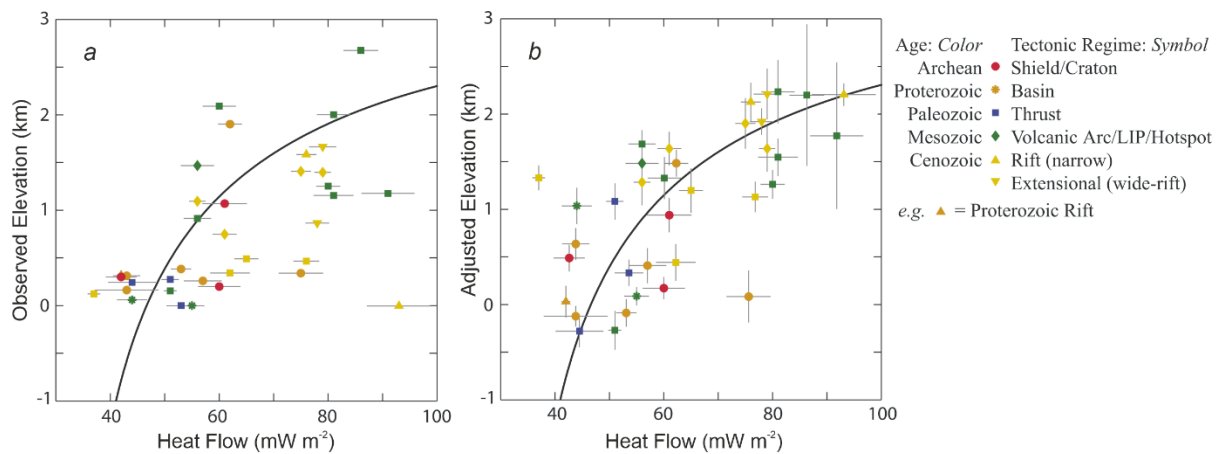
492 et al., 2019). By kriging the heat flow measurements of the continents in their pre-Gondwana breakup  
493 arrangement, Pollett et al. (2019) interpolated a heat flow surface through Antarctica and its conjugate margins  
494 (Fig. 11). This method highlighted similarities and differences between the most recent seismic and magnetically  
495 derived geophysical models of Antarctic heat flow (An et al., 2015b; Martos et al., 2017) with the better  
496 constrained heat flow of the conjugate margins. In particular, this approach showed reasonable agreement along  
497 the margin with Africa, but an absence in either the magnetic or seismic models of high heat flow provinces in  
498 East Antarctica comparable with south Australia; an absence of the low heat flow of SW Australia in the  
499 magnetically-derived model of East Antarctica (Martos et al., 2017); and an absence of the high heat flow of  
500 northern India in the seismically-derived model of East Antarctica (An et al., 2015b). However, when  
501 extrapolating heat flow away from the conjugate margins into the interior of Antarctica, this approach is  
502 susceptible to the method of interpolation used and the quality and scarcity of the borehole-derived GHF estimates  
503 in the interior of Antarctica (Section 3).



504  
505 **Fig. 11. Interpolated heat flow map of Gondwana, showing the derivation of Antarctic GHF from the reconstructed**  
506 **conjugate margins of the supercontinent. Terrestrial heat flow data shown by points. Adapted from Pollett et al. (2019).**

#### 507 4.5. Isostatic elevation

508 In addition to crustal thickness and density, the thermal state of the lithosphere also contributes to its isostasy and  
509 observed surface elevation. The effect of thermal isostasy on the bathymetry of oceanic crust is well recognised:  
510 as oceanic crust migrates from the spreading ridge it cools, thickens, contracts, and subsides (Stein and Stein,  
511 1992). However, the effect of thermal isostasy on continents is masked by compositional contributions to isostatic  
512 elevation (i.e. lateral variations in crustal thickness and density, Fig. 12a; Hasterok and Chapman, 2007b, 2007a).



513

514 **Fig. 12. Relationship of the median observed (a) and adjusted (b) elevation and median compiled heat flow values of 36**  
 515 **geological provinces on the land and continental shelves of North America, ranging from 30 - 2082 x 10<sup>3</sup> km<sup>2</sup>. Compiled**  
 516 **heat flow data excluded values outside of the range 20 - 120 mW m<sup>-2</sup> as these values were most likely affected by near**  
 517 **surface processes (e.g. hydrothermal circulation) or shallow magmatism, and do not reflect the lithosphere's thermal**  
 518 **state. Observed elevations are converted to adjusted elevation by normalising according to their seismically-derived**  
 519 **crustal thickness and crustal density and an equation for thickness and density-based isostasy. The black curve shows**  
 520 **the best-fitting thermal-isostatic model for North American adjusted elevation and heat flow. Adapted from Hasterok**  
 521 **and Chapman (2007a).**

522 Hasterok and Chapman (2007b, 2007a) developed a methodology for investigating thermal isostasy in the  
 523 continental lithosphere by normalising the observed elevation using an isostatic correction. The calculated  
 524 compositionally-corrected elevation generally increases with increasing surface heat flow (Fig. 12b). This  
 525 approach was used to derive the thermal contribution to isostatic elevation of Australia and North America, and  
 526 estimate the continental sub-lithospheric and radiogenic heat flow (Hasterok and Chapman, 2007b; Hasterok and  
 527 Gard, 2016). Whilst in general, the compositionally-corrected elevation and surface heat flow values followed the  
 528 modelled curve for thermal isostatic equilibrium (Fig. 12b), anomalous regions lie away from this curve. These  
 529 anomalies result from: 1) additional sources of buoyancy and/or dynamic support (e.g. anomalously buoyant  
 530 mantle lithosphere); 2) anomalous surface heat flow, not representative of the deeper thermal regime (e.g. high  
 531 concentration of heat producing elements in the shallow crust); 3) deviations from the thermal properties of the  
 532 reference crustal model (e.g. heat production); or 4) combinations of these properties (Hasterok and Gard, 2016).

533 Although developed for regions of known heat flow, application of this approach to Antarctica (Hasterok et al.,  
 534 2019) may provide an alternative estimate of heat flow based largely on two well-constrained variables: surface  
 535 and bedrock topography. However, it is dependent on the quality of constraints on crustal thickness, density, heat  
 536 production, and thermophysical properties of the upper crust (of which uncertainty in upper crustal heat production  
 537 has the largest effect; Hasterok and Chapman, 2007b). For example, regions where high surface heat flow is  
 538 dominantly from anomalously high upper crustal heat production will have lower elevations than regions of  
 539 similar surface heat flow but with lower upper crustal heat production. Crust that has experienced tectonic and  
 540 magmatic activity in the Cenozoic (i.e. <66 Ma) may be in a transient rather steady-state thermal regime, so this  
 541 approach may have challenges in West Antarctica. Steady-state thermal modelling is thus more applicable to the  
 542 old, stable crust of East Antarctica; particularly if the heat flow and isostasy of the conjugate margins are  
 543 considered (Hasterok and Gard, 2016; Pollett et al., 2019). However, differences between the crustal thickness

544 based on gravity modelling and isostatic elevation modelling may indicate variable densities and/or compositions  
545 of the underlying mantle (Pappa et al., 2019b, 2019a).

#### 546 4.6. Enhancement of GHF estimates by incorporation of heterogeneous crustal compositions

547 The geophysical approaches described above assume laterally homogenous heat production in the crust. However,  
548 given the geologically heterogeneous composition of the crust, it is important to consider the effects of variable  
549 lithospheric heat production and incorporate this into forward models of GHF.

550 Radiogenic heat production in the upper crust contributes an estimated 26-40 % of the total continental GHF  
551 (Artemieva and Mooney, 2001; Hasterok and Chapman, 2007b, 2011; Pollack and Chapman, 1977; Vitorello and  
552 Pollack, 1980). Radioactive isotopes of the heat producing elements (HPEs) uranium, thorium, and potassium (U,  
553 Th, and K) are responsible for ~98% of lithospheric heat production (Beardsmore and Cull, 2001). These elements  
554 are incompatible with mineral structures in the mantle and lower crust, so concentrate in the upper crust and  
555 decrease in abundance with depth during planetary differentiation (the chemical and physical separation of an  
556 initially homogenous planetary body into one with an iron-rich core, magnesium-silicate-rich mantle, and a thin  
557 silicate-rich crust; Roy et al., 1968; Rudnick and Fountain, 1995).

558 The upper crust itself is highly heterogeneous in composition. HPE distribution is determined by their  
559 compatibility in different minerals, concentrating them in Si-rich silicic rocks (e.g. granite or rhyolite) relative to  
560 Fe-rich mafic rocks (e.g. gabbro or basalt). Immature sediments inherit the HPE abundance of their eroded source  
561 rocks, but decrease in HPE abundance with increasing maturity and the consequent decrease in their lithic contents  
562 (Burton-Johnson et al., 2017; Rybach, 1986). Crustal heat production is thus heterogeneous, and the most  
563 significant control of HPE abundance and resultant heat production in the lithosphere is the distribution of the  
564 composite lithologies of the upper crust (Lachenbruch, 1968; Sandiford and McLaren, 2002; Taylor and  
565 McLennan, 1985).

##### 566 4.6.1. Whole rock geochemical analysis of heat production

567 Heat production of exposed lithologies can be determined from their concentrations of HPE (U, Th, and K)  
568 determined by geochemical analysis, or by airborne or ground-based gamma ray surveys. Radiogenic heat  
569 production for each sample ( $H$ ,  $\mu\text{Wm}^{-3}$ ) for the present day ( $t=0$ ) can be determined from Equation 7 (Turcotte  
570 and Schubert, 2014):

$$571 \quad H = (0.9928C_0^U H^{U238} + 0.0071C_0^Th H^{Th232} + 0.000119C_0^K H^{K40})D$$

572 (7)

573 Where  $C_0^U$ ,  $C_0^{Th}$  and  $C_0^K$  are the measured concentrations (ppm) of U, Th and K respectively;  $H^{U238}$ ,  $H^{U235}$ ,  $H^{Th232}$   
574 and  $H^{K40}$  are the heat productivities of the respective isotopes  $^{238}\text{U}$  ( $9.37 \times 10^{-5} \text{ Wkg}^{-1}$ ),  $^{235}\text{U}$  ( $5.69 \times 10^{-4} \text{ Wkg}^{-1}$ ),  
575  $^{232}\text{Th}$  ( $2.69 \times 10^{-5} \text{ Wkg}^{-1}$ ) and  $^{40}\text{K}$  ( $2.79 \times 10^{-5} \text{ Wkg}^{-1}$ ); and  $D$  is the assumed density of the rock (e.g. 2800, 2850,  
576 and  $3000 \text{ kg m}^{-3}$  for felsic, intermediate, and mafic granulites, respectively; Hasterok and Chapman, 2011). When  
577 using geochemical data to calculate heat production, this allows new and archive data to be used to calculate the  
578 heat production of the sampled outcrop. However, many archive analyses occurred prior to the development of

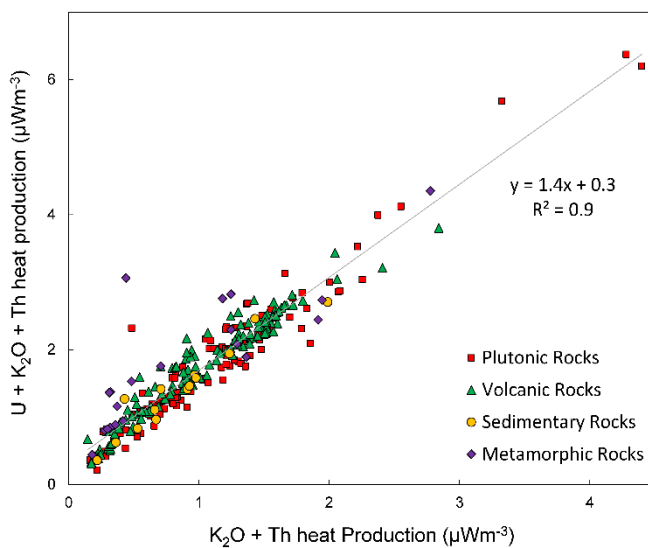
579 accurate U quantification (e.g. by high resolution XRF or ICP-MS). An empirical relationship (Equation 8;  
580 Burton-Johnson et al., 2017) allows calculation of total U, Th, and K heat production ( $H$ ) from samples possessing  
581 only Th and K data ( $H_{K,Th}$ ; correlation coefficient,  $R^2 = 0.9$ ; Fig. 13).

$$582 \quad H = 1.4H_{K,Th} + 0.3$$

583 (8)

584 Heat production values can be assigned to bedrock geology either by interpolation of the point values or by  
585 assigning the point values to the mapped geology and assigning their average value to the geological unit; the  
586 average being either the mean (Veikkolainen and Kukkonen, 2019), area weighted mean (Slagstad, 2008), or  
587 median value (Burton-Johnson et al., 2017). Interpolation shows spatial variability within a unit, but is affected  
588 by the interpolation method used, requires sufficient and evenly distributed data coverage, and is affected by  
589 anomalous values. For these reasons, the median values were used for the unevenly distributed archive data of the  
590 Antarctic Peninsula (Burton-Johnson et al., 2017). In Antarctica, maps of median (Antarctic Peninsula, Fig. 6;  
591 Burton-Johnson et al., 2017) and transects of mean (coastal East Antarctica; Carson et al., 2014; Carson and  
592 Pittard, 2012) heat production data have been integrated with geophysical models of the deeper heat flow to  
593 estimate the total GHF at the bedrock surface.

594 Integrating spatially variable upper crustal heat production into the geophysical models of Antarctic GHF resulted  
595 in increased estimated spatial GHF variability, including local regions of high GHF above HPE-enriched granitic  
596 intrusions (Carson et al., 2014; Leat et al., 2018). The relative concentration of the HPE into the upper crust may  
597 result in it contributing a highly variable 6-70% of the total GHF, although 3D crustal modelling is required to  
598 constrain its thickness (Burton-Johnson et al., 2017). This modelling also showed the impact of sedimentary basins  
599 on GHF distribution, as thick, extensive units of immature, clay-rich sediments may form extensive regions of  
600 enhanced GHF, even though more mature, quartz-rich sediments are associated with low GHF (Burton-Johnson  
601 et al., 2017). This highlights the importance of accurately constraining the upper crustal geology and its chemistry  
602 when estimating GHF from geophysical data.



603

604 **Fig. 13. The relationship between total calculated heat production from U, K<sub>2</sub>O and Th decay and the heat production**  
605 **values from K<sub>2</sub>O and Th only for different broad lithologies, enabling total heat production calculation from incomplete**  
606 **archive data (n = 319; Burton-Johnson et al., 2017).**

#### 607 **4.6.2. Glacially-derived rock clasts**

608 Although heat production can be determined for exposed bedrock, the likely heat production of the rocks beneath  
609 the Antarctic ice sheet is harder to constrain. To investigate East Antarctica, glacial clasts were sampled from  
610 moraines adjacent to the Transantarctic Mountains (Goodge, 2018). Granitic samples older than 500 Ma (Ross  
611 Orogen) were selected as likely lithologies of the interior of East Antarctica, as these are the dominant lithologies  
612 of other Precambrian cratons (>542 Ma regions of tectonically-stable continental crust; e.g. central Canada). These  
613 clasts were analysed for their HPE abundance and attributed to their likely source area (the drainage basin of their  
614 associated glaciers). A probable range of subglacial heat flow values was estimated by assuming mantle and lower  
615 crustal GHF values and a thickness for the upper crust based on other Precambrian shields. This indicates that  
616 East Antarctic heat flow is comparable to other Precambrian cratons, and comparable to geophysical models of  
617 East Antarctic heat flow (Van Liefferinge and Pattyn, 2013). However, broader application of this approach is  
618 biased towards more erosion resistant rock types, whilst less competent lithologies will not be preserved after  
619 glacial transport and deposition.

#### 620 **4.6.3. Gamma ray spectrometry**

621 Rather than whole rock geochemical analysis, the gamma ray spectrum can be used to determine the  
622 concentrations of radioactive isotopes, including those of K, Th, and U, and was first used for U exploration.  
623 Gamma ray spectrometry can be surveyed in the field, on samples, or from the air. Airborne surveys can cover  
624 large areas, and have been used to survey Western Australia, SW England, and all of Finland (Beamish and Busby,  
625 2016; Bodorkos et al., 2004; Hyvönen et al., 1972). However, the data requires multiple corrections, and the  
626 recorded data integrates the radiation from the bedrock, surface cover (including soil and vegetation), the  
627 atmosphere, cosmic radiation, and the aircraft, making the data less accurate than ground measurements or sample  
628 analysis (Veikkolainen and Kukkonen, 2019). The technique is only sensitive to the upper 25cm of the land  
629 surface, with overlying sediments and water bodies masking the radiation and leading to underestimates of heat  
630 production (Phaneuf and Mareschal, 2014). However, if the signal could be linked to mapped geological units and  
631 other evidence for subglacial geology (e.g. aeromagnetic and gravity anomalies) it may be feasible to extrapolate  
632 the calculated heat production beneath the ice sheet. Hand-held gamma ray spectrometry studies, where heat  
633 production can be correlated with lithology along exhumed crustal profiles, show promise in this regard elsewhere  
634 (Alessio et al., 2018).

#### 635 **4.6.4. Crustal structure**

636 Whilst surface HPE distribution can be constrained by measurements, the vertical distribution is more ambiguous.  
637 In heat flow models, heat production is often assumed to decrease exponentially with depth (e.g. Fox Maule et al.,  
638 2005; Martos et al., 2017). This exponential model was developed to explain observations from exposures of  
639 large, thick composite granite bodies (batholiths) where magma was initially emplaced at different depths in the  
640 crust (Lachenbruch, 1968, 1970; Swanberg, 1972) and reflects a proposed decrease in HPE abundance with

641 increasing metamorphic grade (Lachenbruch, 1968; Sandiford and McLaren, 2002). However, this relationship  
 642 has been challenged by other studies comparing HPE abundance and metamorphic grade (Alessio et al., 2018;  
 643 Veikkolainen and Kukkonen, 2019), showing that the lithological change from the largely silicic upper crust to  
 644 the mafic lower crust has a larger influence on HPE abundance than metamorphic grade (Bea, 2012; Bea and  
 645 Montero, 1999). Deep (9-12 km) boreholes also show a correlation of heat production with lithology, but not with  
 646 depth (Clauser et al., 1997; Popov et al., 1999). In fact, heat production *increased* for the first 2 km of the 12 km  
 647 superdeep well of the Kola Peninsula, Russia, then remained variable but high with increasing depth (Popov et  
 648 al., 1999). Similarly, heat production increases below 3 km in the recent 5 km UD-1 well of the Cornubian  
 649 Batholith, UK (Dalby et al., 2020). As such, the available evidence indicates that the first-order HPE distribution  
 650 is controlled by the HPE abundance of the crust prior to metamorphism and the vertical distribution of the crust's  
 651 composite rock types. Inversely, it indicates that HPE distribution is not controlled by depth in the crust or the  
 652 degree of metamorphism resulting from the increase in pressure and temperature.

653 Without evidence for the deeper structure of the crustal column, the lithological and HPE distribution of the  
 654 lithosphere can instead be modelled as layers of variable thickness and heat production: the upper crust, middle  
 655 crust, lower crust, and mantle lithosphere. Surface heat flow is largely insensitive to variations in the heat  
 656 production or thickness of the mafic lower crust and mantle lithosphere due to their heat production being ~1-2  
 657 orders of magnitude lower than that of the upper crust (Hasterok and Chapman, 2011; Rudnick and Fountain,  
 658 1995; Rudnick et al., 1998). The middle crustal layer can either be excluded (Hasterok and Chapman, 2011) or  
 659 treated as a layer of invariable heat production (e.g. An et al., 2015, for Antarctica) due to its low heat production  
 660 compared with the range of the upper crust. Lithospheric heat production can thus be defined by the heat  
 661 production and relative thickness of the upper crust, or upper crustal heat producing layer (Hasterok and Chapman,  
 662 2011). This can be defined by:

$$663 \quad Q_s = Q_b + H_{UC}D = FQ_s + H_{UC}D = H_{UC}D/(1 - F)$$

664 (9)

665 Where  $Q_s$  is the surface heat flow,  $Q_b$  is the basal heat flow of the upper crust,  $H_{UC}$  is upper crustal heat production,  
 666  $D$  is the thickness of the upper crustal heat producing layer, and  $F$  is the proportion of the surface heat flow  
 667 contributed by the basal heat flow ( $Q_b$ ) (adapted from Hasterok and Chapman, 2011).

668 Rather than a simple layered model, more complex 2D or 3D models of upper crustal structure can be developed  
 669 using geophysical data, and the 2D or 3D crustal units assigned heat production and conductivity values based on  
 670 analyses of representative exposures. A 3D crustal model derived from gravity and aeromagnetic data was  
 671 developed to map heat flow in Norway (Ebbing et al., 2006; Olesen et al., 2007). In Antarctica, this has been  
 672 applied in 2D to the high heat production granites of the Ellsworth-Whitmore Mountains using airborne magnetic  
 673 and gravity data and bedrock topography (Leat et al., 2018), and the Transantarctic Mountains using topography  
 674 and satellite gravity data (Pappa et al., 2019b).

675 Even though variability in deep lithospheric heat production has a smaller effect on surface heat flow than  
 676 variability in upper crustal heat production (Hasterok and Chapman, 2011), it is not homogenous. These  
 677 thermophysical properties can be constrained from deep xenoliths (fragments of rock entrained in magma rising

678 from depth) (Hasterok and Chapman, 2011; Martin et al., 2014) and crustal sections (Berg et al., 1989), which  
679 can also inform on the local geothermal gradient at the time of their crystallisation.

680 To help constrain the properties of the Antarctic mantle, including its influence on Antarctic heat flow, a  
681 Geological Society of London Memoir is currently being compiled summarising the data gained from mantle  
682 xenoliths (Martin and van der Wal, in prep.). This includes a sample database, and a compilation of their grain  
683 size and water content. These xenoliths are from shallow sources, as their occurrence is biased towards areas of  
684 crustal rifting where the lithosphere is thinner, although some xenoliths are from deeper sources (e.g. from the  
685 Amery Rift and Ferrar Dolerite).

## 686 **5. Glaciological inverse estimation of GHF**

687 Although geothermal heat flow has a geological derivation, it can also be constrained by multiple approaches  
688 through its observable effects on the overlying ice sheet. Inverse modelling can be applied to observed  
689 glaciological properties (e.g. glacial flow and melt rates) and the required GHF calculated. We will describe in  
690 this section different methods used in glaciology to derive GHF.

### 691 **5.1. Subglacial water**

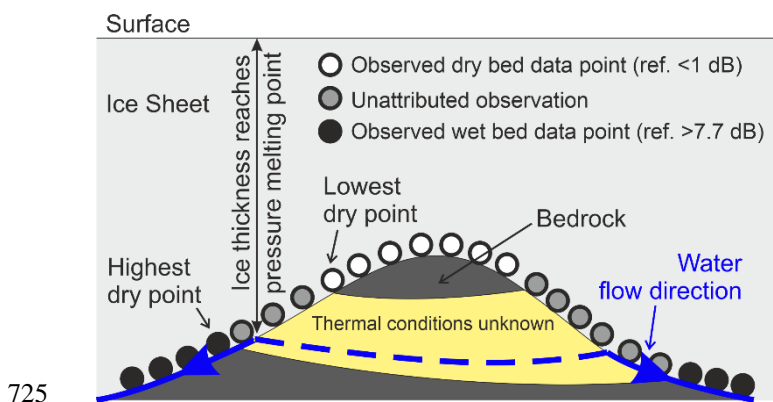
692 The presence of subglacial water can be detected with an ice-penetrating radar. The reflective properties of the  
693 ice-bedrock interface depend on the presence of water and, with certain caveats, radar surveys can be used to map  
694 subglacial water. In general terms, a glaciological model can then be used to estimate the values of GHF that  
695 better predict where basal temperatures reach the pressure melting point and melting occurs. We will describe in  
696 this Section examples of this approach.

697 Carter et al. (2009) modelled the dielectric loss of radar data through the ice column around Dome C in East  
698 Antarctica (Fig. 6) to infer the basal reflectivity and verify the presence of subglacial water. Because the  
699 temperature profile of the ice sheet is one parameter affecting dielectric loss, this approach required inference of  
700 the basal heat flow from temperature-depth modelling over the last 254 ka. The Shapiro and Ritzwoller (2004)  
701 GHF model was used initially (see section “4.2. Seismic estimates”), but when the calculated vertical ice velocity  
702 ( $m_w$ ) at the bed exceeded the initial melt rate ( $m_T$ ), the GHF was modified until  $m_T$  and  $m_w$  were equal. This  
703 approach identified localised high GHF anomalies, but (excepting these anomalies) they calculated that 66 % of  
704 the study area was either at or near the pressure melting point (anywhere that ice is thicker than 3500 m) without  
705 invoking enhanced GHF.

706 Schroeder et al. (2014) modelled the spatial distribution of melt beneath the ice sheet in the Thwaites Glacier  
707 catchment (Fig. 6) by mapping the relative bed echo strength of radar data in the region and modelling the water  
708 routing required to match these observations by routing alone (without heterogeneous basal melting). These  
709 routing models were based on the radar-derived ice thickness and surface slope. The 50 selected routing models  
710 were used to model the relative melt required to reproduce the observed echo strengths of each routing model.  
711 This relative melt model was in turn scaled to match the total melt water produced in an ice sheet model of the  
712 Thwaites Glacier incorporating frictional melting, horizontal advection, and an assumed uniform GHF. By  
713 subtracting the frictional and advective contributions, the GHF required to produce the remaining melt could be

714 calculated. This approach predicted very high heat flow in this region (114 to >200 mW m<sup>-2</sup>), with the highest  
715 heat flow focused around observed and inferred subglacial volcanoes.

716 With the aim of determining appropriate sites of low basal melting for old-ice drilling, Passalacqua et al. (2017)  
717 also used radar evidence for basal melting and ice sheet modelling to determine GHF around Dome C (Fig. 6).  
718 Wet and dry bed conditions were identified from radar data and ten spots were identified on bedrock topographic  
719 features marking the critical ice thickness where present basal melting becomes possible. These spots were defined  
720 as locations where the upper slopes of the bedrock topography are dry and their lee slopes are wet, with melting  
721 initiating between the two when the ice thickness passes the pressure melting point (Fig. 14). Assuming that GHF  
722 is locally homogeneous between the two bedrock elevations, heat flow was determined by increasing its value in  
723 a 1-D heat model of the local ice thickness until basal melting occurred. These point estimates were interpolated  
724 to generate an approximate map of regional heat flow and calculate basal melt rates over the last 400 ka.



725  
726 **Fig. 14. Illustration of how the ice thickness exceeding the pressure melting point (PMP) can be identified from radar**  
727 **reflectivity data points, indicating the presence or absence of basal water beneath the ice sheet. Once the PMP is**  
728 **identified, thermal modelling can estimate the required local GHF. Between the thresholds of radar reflectivities**  
729 **representative of wet and dry basal conditions, the thermal conditions are unknown (yellow-shaded region of the**  
730 **bedrock). Adapted from Passalacqua et al. (2017).**

731 Van Liefferinge and Pattyn (2013) and Van Liefferinge et al. (2018) used steady state and transient  
732 thermodynamic modelling of the East Antarctic Ice Sheet to map the minimum heat flow required to raise the  
733 basal temperature above pressure melting point and generate basal melting. Whilst this was executed to identify  
734 possible sites for drilling the oldest ice in areas that are unlikely to have undergone basal melting in the last 1.5  
735 Ma and did not produce an estimate of absolute GHF, if this approach were combined with other evidence for  
736 basal conditions above the pressure melting point (e.g. combining thermodynamic modelling with subglacial lake  
737 locations), points of minimum heat flow could be mapped.

## 738 5.2. Subglacial lakes

739 If temperatures are sufficient for basal melting, and topography depressions are suitable, subglacial lakes can  
740 develop. Subglacial lakes exhibit radio reflectivities 10-20 dB greater than the ice-bedrock boundary, allowing  
741 the current identification of at least 402 lakes beneath the Antarctic ice sheet (Wright and Siegert, 2012).

742 Whether basal temperatures are sufficient for basal melting and preservation of subglacial lakes is dependent on  
743 ice thickness, the surface temperature and accumulation rate, heat transported through ice advection, heat  
744 produced by internal deformation and basal sliding, and the GHF. When subglacial lakes are located near ice  
745 divides, heat derived by horizontal advection, basal friction, and internal deformation is assumed to be minimal,  
746 and thus the heat required to bring the base of the ice sheet above the pressure melting point is a product of ice  
747 thickness and GHF. Thus, when subglacial lakes are located near ice divides and the accumulation rate is known  
748 (high accumulation rates cool the ice mass), point estimates of *minimum* GHF can be calculated from one-  
749 dimensional thermal models of the ice sheet temperature profile, but an assumption that water was derived locally  
750 and not routed from elsewhere must also be considered as lakes can only form in topographic depressions. The  
751 absence of a lake or basal water does not imply the bed is frozen if the water can drain away (Pattyn, 2010; Siegert  
752 and Dowdeswell, 1996).

753 Conversely, and with the same caveats regarding basal topography and drainage, where the ice sheet is known to  
754 be frozen to the bed, the *maximum* GHF can be estimated. For example, Fudge et al. (2019) used the presence of  
755 Raymond Arches to deduce where the ice was frozen to the bed at the Siple Coast ice rises to estimate maximum  
756 GHF values. Combined, maximum and minimum estimates are more useful than either alone.

### 757 5.3. Englacial stratigraphy

758 Jordan et al. (2018) identified draw down of internal ice sheet layers and increased bed reflectivity from radar data  
759 ~200 km from the South Pole (Fig. 6), indicating enhanced basal melting. Melt rates were calculated using dated  
760 radar layers, traced from the Dome C ice-core site, and a depth age model that simulates the draw-down effect of  
761 ice from subglacial melt rate. The low ice velocity ( $<1.5 \text{ m a}^{-1}$ ) indicated minimal frictional contribution to basal  
762 temperature, and a location at the top of a hydraulic catchment area indicated a low heat contribution from  
763 subglacial water. By negating these contributions to heat flow, assuming the basal temperature is at the pressure  
764 melting point (and thus could be derived from the ice thickness) and that temporal temperature variations match  
765 those of the Dome C ice core, a time-dependent heat equation was applied to the ice sheet to derive the basal GHF  
766 required to generate the enhanced melt rates.

### 767 5.4. Microwave emissivity

768 Englacial temperature profiles have been derived from satellite and airborne passive detection of high frequency  
769 L-band microwave radiation (~1.4 GHz; Macelloni et al., 2019, 2016; Passalacqua et al., 2018); data primarily  
770 collected to investigate soil moisture and ocean salinity (Kerr et al., 2010). These wavelengths have very low  
771 absorption in ice and low scattering by particles (e.g. grainsize and ice bubbles), providing high penetration depths  
772 in dry ice.

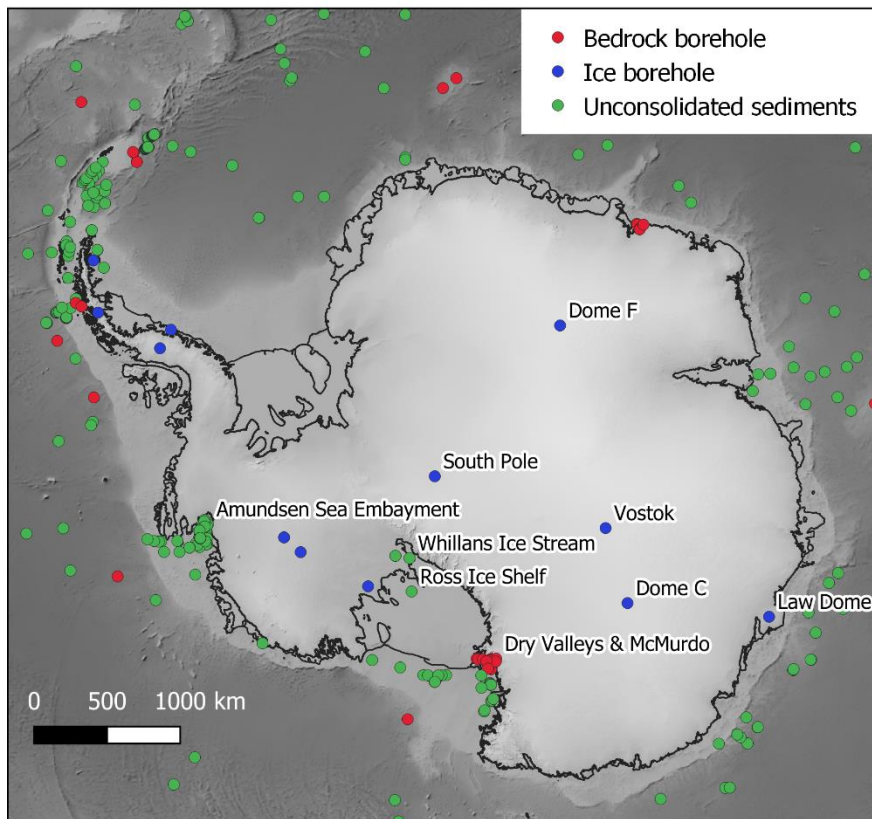
773 Macelloni et al. (2019) derived englacial temperature profiles for the Antarctic ice sheet from 2-year averaged  
774 vertical-polarised (V) radiation collected at the “Brewster angle” ( $57.1^\circ \pm 2.6^\circ$ ; the angle of incidence at which the  
775 radiation is perfectly transmitted through the air-snow interface with no reflection, minimising the influence of  
776 surface or shallow sub-surface effects). The corrected intensity (brightness temperature,  $T_B$ ) correlates with the  
777 surface temperature of the ice, but is also affected by the ice sheet thickness (a largely inverse correlation), density  
778 profile, and grain size (Macelloni et al., 2016). As such, the ice sheet’s thermal structure at depth could be

779 estimated by comparing the observed  $T_B$  and a simulated  $T_B$  derived through microwave emissivity modelling,  
780 including one-dimensional modelling of the ice sheet's temperature profile. Included in the assumed values for  
781 this modelling are the GHF and the accumulation rate; the sources of greatest uncertainty. This method only  
782 applies in areas of slow flowing ice ( $<10 \text{ m yr}^{-1}$ ), and is optimal in areas of very slow flowing ice ( $<5 \text{ m yr}^{-1}$ ) as  
783 this negates heating by horizontal ice advection and deformation-derived heat production. It is also only applicable  
784 to areas of thick ice ( $>1000 \text{ m}$ ) as the simulations used to model microwave emission do not include bedrock  
785 reflections. This is not a limitation for application to Antarctic GHF research, as it is under these conditions that  
786 heat flow has the greatest influence on ice sheet dynamics.

787 Comparison of the microwave-derived temperature profile and that simulated by glaciological modelling (Van  
788 Liefferinge and Pattyn, 2013) show good agreement in the upper third of the ice sheet, but diverge in their  
789 temperature estimates with depth, with the largest uncertainties close to the bedrock. This is largely due to  
790 uncertainty in the GHF, but also reflects a decrease in sensitivity of the simulated  $T_B$  to the temperature profile  
791 below 1000-1500 m (the bottom 1000-1500 m of the ice sheet contributes  $<10 \%$  to the total emission). Longer  
792 wavelength emissions (0.5 GHz) with greater sensitivity to the deeper temperature profile may provide greater  
793 accuracy at depth (Jezek et al., 2014). Deep measurements of the ice sheet's temperature profile are required to  
794 validate this method compared to the glaciological models. Although currently limited by its sensitivity to  
795 temperature at depth and the accuracy of the assumed parameters (notably accumulation rate), this approach has  
796 the potential to constrain basal heat flow through variation of the assumed GHF values used in the emissivity  
797 modelling.

## 798 **6. Existing data**

799 Although subglacial borehole-derived estimates of terrestrial GHF are lacking in Antarctica, estimates have been  
800 made from probes into marine sediments and boreholes into exposed bedrock. We have compiled 431 of these  
801 point estimates (Fig. 15; data available in the Supplementary Material and from  
802 <https://github.com/RicardaDziadek/Antarctic-GHF-DB>). The compiled data originates from multiple methods,  
803 and is variable in its accuracy and limitations, and so we have attempted to qualitatively grade the likely reliability  
804 of each estimate based on specific parameters (Supplementary Material). We do not include values for marine  
805 measurements compiled in the database "Global Heat Flow Data – Abbott Compilation". This database is  
806 available via GeoMapApp and completely undocumented. The labels may point to cruise reports, but not  
807 published data and the data quality remains impossible to evaluate up to this point.



808

809 **Fig. 15. Locations of all compiled point estimates of GHF. Database available in the Supplementary Material and from**  
 810 <https://github.com/RicardaDziadek/Antarctic-GHF-DB>.

### 811 6.1. Boreholes into bedrock

812 Terrestrial, borehole-derived measurements of the geothermal gradient (12 boreholes, Supplementary Material)  
 813 are limited to the Dry Valleys and McMurdo Sound region (Fig. 15; Bucher, 1980; Decker, 1974; Decker and  
 814 Bucher, 1982; Pruss et al., 1974; Talalay and Pyne, 2017), and no subglacial terrestrial borehole measurements  
 815 have been made into the Antarctic bedrock. However, as discussed in Section 3.1., temperature gradients in  
 816 bedrock must be taken to a sufficient depth to be representative of upward conduction of the GHF rather than  
 817 downward conduction of the surface temperature. Whilst the GHF estimates from the Dry Valleys Drilling Project  
 818 (DVDP, including McMurdo Station) were taken from the 75 to >300 m deep boreholes (Bucher, 1980; Decker  
 819 and Bucher, 1982; Talalay and Pyne, 2017), the shallow 7.6 m borehole from McMurdo Station produces a much  
 820 higher GHF estimate ( $164 \text{ mW m}^{-2}$ , Risk and Hochstein, 1974). This shallow measurement should thus be  
 821 neglected in preference for the  $66 \text{ mW m}^{-2}$  value from the 260 m deep DVDP borehole (Decker and Bucher, 1982).

822 Boreholes into submarine bedrock (34 boreholes, Supplementary Material) have been drilled and temperature  
 823 gradients measured beneath the McMurdo Sound, Amundsen Sea Embayment, and Ross Ice Shelf (Fig. 15;  
 824 Bückler et al., 2001; Decker et al., 1975; Gohl et al., 2019; McKay et al., 2018; Morin et al., 2010).

825 The US Rapid Access Ice Drill project (RAID) aims to achieve the first subglacial, borehole-derived thermal  
 826 measurements of bedrock following drilling of the overlying ice sheet and coring of  $\geq 25$  m of bedrock (Godge  
 827 and Severinghaus, 2016).

## 828 6.2. Ice boreholes

829 GHF estimates from ice boreholes (15 boreholes, Supplementary Material) are better distributed across the  
830 Antarctic continent than terrestrial bedrock boreholes (Fig. 15). However, not all ice boreholes drilled have been  
831 sufficiently deep or in appropriate sites for GHF estimation (i.e. the ice sheet needs to be stationary and frozen to  
832 the bed). This limits the available GHF estimates to Vostok (Salamatin et al., 1998), Law Dome (Dahl-Jensen et  
833 al., 1999), South Pole (Price et al., 2002), Marie Byrd Land (Clow et al., 2012; Engelhardt, 2004; Gow et al.,  
834 1968), and the Antarctic Peninsula (Mulvaney et al., 2012; Nicholls and Paren, 1993; Zagorodnov et al., 2012)  
835 (Fig. 15). Dome Fuji (Hondoh et al., 2002) is not frozen to the bed, but provides a minimum GHF estimate.

## 836 6.3. Marine and onshore unconsolidated sediments

837 The most abundant resource of heat flow estimates from measured temperature profiles around Antarctica comes  
838 from unconsolidated marine sediments (Fig. 15; 362 measurements south of  $-72^{\circ}$  S, Supplementary Material).  
839 However, the data distribution is sparse and heterogeneous, and whilst some regions are well sampled (e.g. the  
840 Amundsen Sea embayment; Dziadek et al., 2019, 2017), other regions (e.g. the Weddell Sea) remain poorly  
841 constrained (Fig. 15). In addition to the open water measurements, two shallow probes (deepest sensors at 1.4 and  
842 0.8 m below the upper sediment surface) have measured the temperature gradient in subglacial sediments below  
843 the Whillans Ice Stream (Begeman et al., 2017; Fisher et al., 2015; see section 3.3.). Two temperature gradients  
844 have also been measured beneath the Ross Ice Shelf (Foster, 1978; Morin et al., 2010), but otherwise heat flow  
845 beneath the Antarctic ice shelves remains poorly constrained regions.

846 As discussed in Section 3.3, when using these estimates it is important to consider whether the shallow ( $< \sim 5$  m)  
847 temperature gradient recorded by the probe is representative of the deeper GHF, or will have been perturbed by  
848 temperature variation in the overlying ice sheet or water column (e.g. Dziadek et al., 2019). Consequently, the  
849 water depth, the temperature profile of the water column, and possible sources of long-term temperature variation  
850 (e.g. variations in deep water circulation and temperature) should be considered when selecting appropriate point  
851 estimates. Similarly, whilst the shallow temperature gradients measured from Subglacial Lake Whillans (Fisher  
852 et al., 2015), and the Whillans Ice Stream grounding zone (Begeman et al., 2017) are presented as subglacial direct  
853 measurements of Antarctic GHF, by the nature of their location within an ice stream they are not in a thermal  
854 steady state, and the temperature profile will have been affected by long term variation from heat advection and  
855 shear heating. These are effects that cannot be evaluated from their very shallow temperature gradient (0.8 and  
856 1.4 m deep), and accordingly these estimates should be used with caution.

## 857 7. Current challenges and future research directions

858 The collated existing data and methodologies presented above highlight our current limitations in determining the  
859 subglacial GHF of Antarctica and allow discussion of future research.

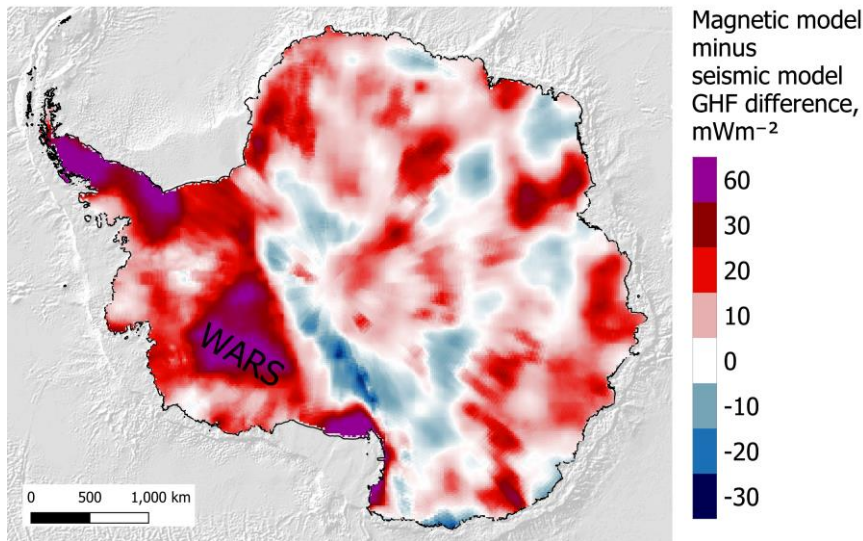
### 860 7.1. Borehole and probe-derived estimates

861 The fundamental limitation for GHF estimation in Antarctica is the lack of borehole-derived estimates from  
862 beneath the Antarctic ice sheet. Without these independent, discrete validation points, the more extensive regional  
863 estimates cannot be accurately evaluated. Therefore, the most promising future development will be the  $\geq 25$  m

864 deep bedrock borehole measurements of the Rapid Access Ice Drill project (RAID; Goodge and Severinghaus,  
865 2016). However, (as noted above) local temperature gradients may not be representative of the regional heat flow,  
866 as local geology, hydrothermal circulation, and topography can result in localised GHF variability. In response,  
867 multiple boreholes where the basal ice is frozen to the bedrock are required to categorise the regional variation,  
868 and topographic effects must be considered and accounted for. Topography may have significant effects on GHF  
869 via its effects on heat diffusion pathways to the surface (Bullard, 1938; Lees, 1910) and must be considered and  
870 investigated in GHF estimates at all scales, including those based on local temperature gradient measurements  
871 (i.e. borehole and probe-derived estimates) and more extensive geophysical and glaciological-derived models.

872 It is also a necessity that thermal modelling of the bedrock temperature profile for the RAID target sites is executed  
873 prior to drilling to constrain the penetration depth of low-frequency time variation of temperature. Whilst the  
874 RAID target bedrock borehole depth of  $\geq 25$  m is much shallower than the  $>100$  m borehole depth achieved for  
875 exposed bedrock (Section 3.1.), the overlying ice sheet insulates the bedrock temperature profile from short  
876 duration surface temperature variability (temperature variation penetration depth is dependent on the frequency  
877 of the variation and thermal diffusivity of the material; Carslaw and Jaeger, 1959). However, as is considered for  
878 GHF estimates from ice boreholes (Section 3.2.), low-frequency variation in surface temperatures, heat advection,  
879 and shear heating will all affect the subglacial temperature profile. Consequently, low-frequency temperature  
880 variation must be corrected for, and boreholes are best drilled where the ice is stationary and frozen to the bed (as  
881 is applied to ice borehole selection for GHF estimation). By drilling in such sites where glaciological approaches  
882 are most effective for GHF estimation, the RAID data will allow validation of GHF estimates for the various  
883 englacial temperature methods applied to stationary ice at ice divides (Section 5.). These methods include borehole  
884 temperature profiles, subglacial lakes, ice sheet models, and microwave emissivity. It is thus important that the  
885 englacial temperature profile is measured in addition to the bedrock temperature gradient.

886 Beyond bedrock drilling there is lot to be gained from further ice borehole drilling. Firstly, existing data must be  
887 evaluated to ensure the methodologies of GHF modelling from borehole temperature profiles are consistent and  
888 accurate. Future ice boreholes into stationary ice frozen to the bed has the potential to supplement the existing  
889 borehole and probe-derived GHF estimates, particularly if the proposed methodology for shallow boreholes can  
890 be validated (600 m depth, or the upper 20% of the ice column; Section 3.2.).

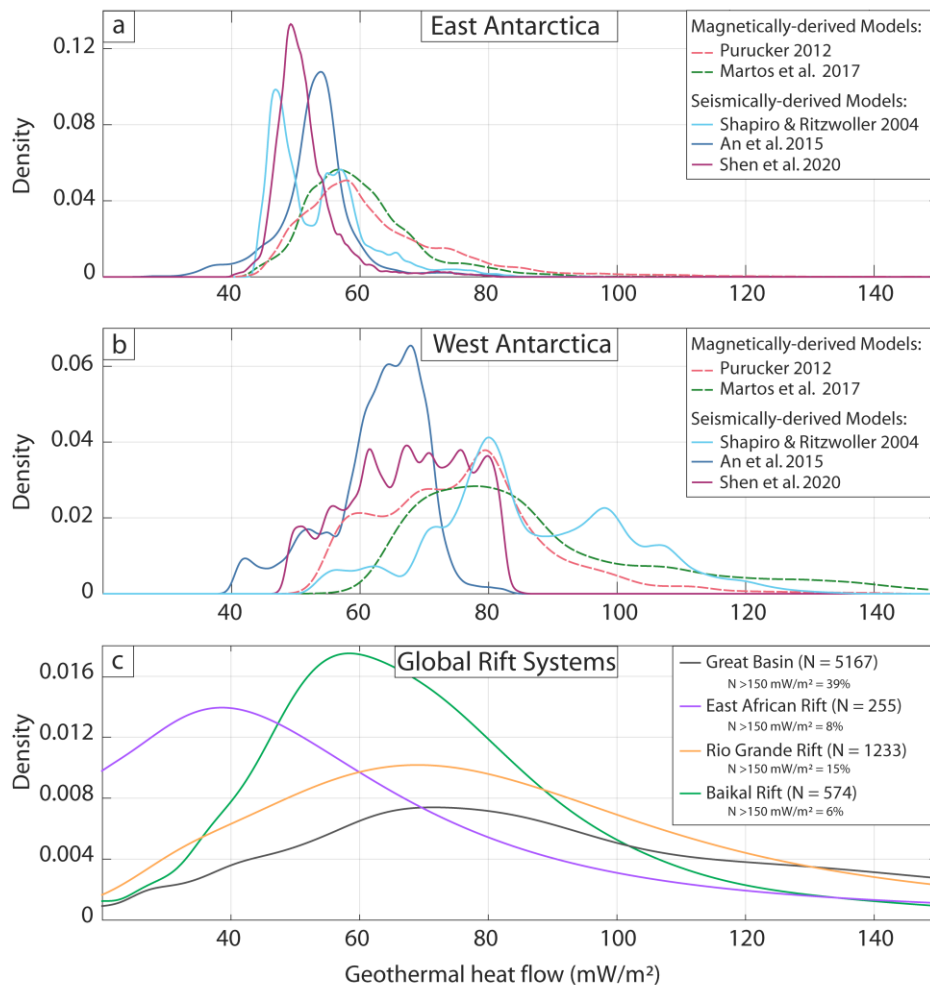


892

893 **Fig. 16. Difference in heat flow values between the most recent magnetic (Martos et al., 2017) and forward-modelled**  
894 **seismic (An et al., 2015b) heat flow models. WARS – West Antarctic Rift System.**

895 Whilst only geophysical methods have provided continental-scale GHF estimates, their values and distribution  
896 vary greatly (Fig. 5, Fig. 16, and Fig. 17). Probability density functions show that whilst there is better agreement  
897 in East Antarctica (Fig. 17a), the seismically derived models estimate more variable and slightly higher GHF than  
898 the magnetically-derived models. In West Antarctica the discrepancies between models are greater (Fig. 5g and  
899 Fig. 17b) even when using similar techniques (compare the empirical seismically-derived estimates of Shapiro  
900 and Ritzwoller, 2002 and Shen et al., 2020, Fig. 17b). However, none of the models of West Antarctica reflects  
901 the GHF distribution of other better-constrained rift systems (Fig. 17c; Lucazeau, 2019), where much more  
902 heterogeneous distributions and a greater proportion of high GHF values ( $>150 \text{ mW m}^{-2}$ ) are expected.

903 The fundamental question thus remains: does the West Antarctic Rift System (WARS) have elevated GHF? The  
904 magnetically-derived model of Martos et al. (2017) estimates high GHF, but the most recent forward and  
905 empirically-derived seismic models do not (An et al., 2015b; Shen et al., 2020; Fig 5). If the seismic models are  
906 correct, then the high GHF estimates of the magnetic model reflect thinning of the magnetic crust, but GHF has  
907 subsequently reduced in the  $\sim 90 \text{ My}$  since the dominant phase of WARS crustal extension in the Cretaceous  
908 ( $\sim 105\text{-}95 \text{ Ma}$ , Siddoway, 2008; as illustrated in Fig. 9b). If the magnetic model is correct, then GHF remains  
909 elevated in response to the younger, 43-11 Ma Cenozoic phase of crustal extension (Granot and Dymant, 2018;  
910 e.g. Fig. 9a). Subglacial hydrological modelling (Schroeder et al., 2014) supports the high GHF estimates in the  
911 Thwaites Glacier region of the WARS. However, high-fidelity borehole estimates, and better constraints on the  
912 nature of the geology, lithospheric architecture, and tectonic history of the WARS are required if we are to resolve  
913 the different estimates and use other locations as analogues for verifying the modelled GHF distribution.



914

915 **Fig. 17. Probability density functions of the geophysically derived continental GHF datasets (Fig. 5 a – e) for a) West**  
 916 **Antarctica and b) East Antarctica. Values extracted at 10 km spacing. The histograms were calculated with a bin size**  
 917 **of 1 and fitted with a non-parametric distribution in the positive domain. c) GHF estimates from measured temperature**  
 918 **gradients for global rift systems for comparison with West Antarctica (data from Lucazeau, 2019). Note the number of**  
 919 **proportion of the data points (N) greater than 150 mW m<sup>-2</sup>.**

920 To evaluate the accuracies of the different models, uncertainty estimates are required. Uncertainties of <10 mW  
 921 m<sup>-2</sup> for the majority of Antarctica were presented for the Curie Depth GHF model of Martos et al. (2017).  
 922 However, not only are the modelled values greatly different from those derived by seismic modelling (An et al.,  
 923 2015b), the calculated Curie depth is deeper than the seismically- or gravitationally-derived Moho depth for large  
 924 areas of the continent (Fig. 10). Even though this can occur where metallic phases are present in cratonic mantle  
 925 (Ferré et al., 2013; Section 4.1.), this cannot explain the full distribution, nor are these occurrences likely to be  
 926 this extensive. Without being critical of the model itself, it is reasonable to dispute the accuracy of the calculated  
 927 uncertainties, and suggest that although their calculation from the geophysical data may be logical, there may be  
 928 a geological contribution to uncertainty (e.g. lithological variation in the lithosphere) that is not being considered.  
 929 As GHF models are utilised by researchers in different fields to those publishing the models, they cannot be  
 930 independently evaluated by the user, and so accuracy in published uncertainty values is arguably more important  
 931 than the accuracy of the model itself. We recommend that future research (including geophysical, geological,  
 932 glaciological, and borehole and probe-derived estimates) is careful in its presentation of uncertainty.

933 The largest limitations to existing geophysical-derived GHF models are uncertainties in the structure,  
934 composition, heat production, and thermophysical properties of the unexposed crust, lithosphere, and underlying  
935 mantle. All current continental models assume the lithosphere to be laterally homogenous in its composition and  
936 thermophysical properties, and although seismic GHF models (e.g. An et al., 2015b) incorporate variable mantle  
937 temperatures, its composition is assumed to be homogenous. Geophysical GHF models assume that lithospheric  
938 heat production is focussed in the upper crust, and is orders of magnitude greater than the deeper heat production  
939 of the middle and lower crust and the mantle. These models assume that lithospheric heat production either  
940 exponentially decreases with depth (e.g. the Curie depth models of Fox Maule et al., 2005; Martos et al., 2017;  
941 and Purucker, 2012) or is concentrated within a laterally homogenous layer of variable depth and constant heat  
942 production (e.g. the seismic model of An et al., 2015a, and the thermal-isostatic model for Australia of Hasterok  
943 and Gard, 2016). However, although the lower crust is enriched in mafic rocks (iron-rich rocks of high  
944 crystallisation temperature, e.g. basalt) of low heat production, deep boreholes and crustal sections have shown  
945 that whilst there is a correlation between heat production and lithology in the upper crust, there is no such  
946 correlation with depth or metamorphic grade (Section 4.6.3.). Similarly, the assumption of laterally homogenous  
947 heat production has been shown to be unreasonable for estimation of Antarctica's GHF, which (like all continents)  
948 has a laterally variable geology and associated concentration of HPEs (Burton-Johnson et al., 2017; Carson et al.,  
949 2014). The exponential decrease model of crustal heat production should thus be rejected, and attempts should be  
950 made to derive the depth and structure of crustal heat production.

951 The most promising approach to address the challenge of uncertainty in the contribution to GHF from the  
952 unexposed crust and deeper lithosphere is the derivation of a three-dimensional lithospheric structure model for  
953 Antarctica. This approach uses geophysical modelling integrating seismic, magnetic, and thermal-isostatic  
954 evidence, and integrating into the modelling the heat production, conductivity, and petrophysical properties of  
955 exposed lithologies and deeper crustal xenoliths or crustal sections. A similar model was developed for Norway  
956 (Ebbing et al., 2006; Olesen et al., 2007), and an Antarctic model would build upon recent 2D and 3D  
957 geophysically-derived models (Leat et al., 2018; Pappa et al., 2019b, 2019a). This requires an expanded database  
958 of the geochemistry of Antarctica's rock outcrops (particularly the HPEs). Beneath the Antarctic ice sheet, where  
959 the surface geology is unknown, the lithologies and probable heat production is best constrained by determining  
960 the probable heat production of each drainage basin based on its detrital clasts (e.g. Goodge, 2018).

961 The assumption of a homogenous mantle composition beneath East Antarctica is challenged by discrepancies  
962 between the Moho depth models derived by gravity and isostatic modelling (Pappa et al., 2019b, 2019a), as this  
963 indicates variable lithospheric mantle densities, or deeper mantle effects on topography. A review of the available  
964 mantle xenoliths and mantle-derived basalt chemistry may be able to constrain the composition of the mantle  
965 beneath Antarctica, and thermal-isostatic modelling may be able to identify these regions of anomalous mantle  
966 anomalies (as in the Australian study of Hasterok and Gard, 2016). If the seismic data for Antarctica is sufficient  
967 to determine crustal density, such a thermal isostatic model would provide an additional independent method to  
968 determine the depth of the upper crustal heat producing layer (Hasterok and Chapman, 2011) and evaluate the  
969 other GHF models.

970 Finally, it is important to compare Antarctica with its conjugate margins (e.g. Pollett et al., 2019), where GHF and  
971 crustal structure are better constrained. This provides constraints on the GHF along the margins of East Antarctica,  
972 as well as informing on the geology beneath the ice sheet.

973 Beyond individual geological and geophysical approaches, a further challenge is how best to integrate different  
974 models. Robust methods must be developed to incorporate datasets with different resolutions and uncertainty,  
975 including techniques already used by the broader data analysis community. For example, Rezvanbehbahani et al.  
976 (2017) applied a multi-variate regression analysis to estimate heat flow in Greenland from sparse and variable  
977 geological and geophysical models and data.

### 978 7.3. Glaciological GHF estimates

979 Englacial temperatures are more sensitive to GHF in areas of the interior of Antarctica where basal sliding is  
980 negligible (Section 2.1). Out of all the methods discussed to derive GHF in the Antarctic interior, the most  
981 promising method is to derive GHF from englacial temperatures obtained from microwave emission (Section 5.4.)  
982 at a longer wavelength (0.5 GHz) than the currently available (~1.4 GHz). The increase in wavelength will reduce  
983 the uncertainty in englacial temperatures below 1000-1500 m (Jezek et al., 2014). By improving the estimations  
984 of englacial temperature near the bed, this will reduce the role of ice flow modelling required to extrapolate  
985 temperature from the partial-depth data. Potentially, if near-the-bed englacial temperatures are known with  
986 sufficient precision, GHF could be derived as from borehole thermometry (Section 3.2). However, the longer-  
987 wavelength method requires the acquisition of currently unavailable satellite-derived data. The method is only  
988 applicable in areas of thick, very slow-flowing ice, and within this area only two ice boreholes exist for validation.  
989 Further validation of the technique to determine the origin of the differences between the temperature model  
990 derived from emissivity data, and glaciological thermal modelling (Macelloni et al., 2019), and other spatially  
991 variable processes affecting microwave emissivity must also be considered (e.g. wind speed, accumulation rate,  
992 surfaces roughness, and density heterogeneities in the firn layer; Passalacqua et al., 2018).

993 Existing glaciological data, like subglacial water distribution or dated englacial layers, has been successfully used  
994 in estimating heat flow in regions of thick, slow flowing ice near ice divides, where advection and shear heating  
995 are minimised. To extend these regional studies to continental scale, both data and models have to be improved.  
996 A significant challenge for radar-derived subglacial water distribution is our ability to discriminate between water  
997 at the bed versus contrasts in the geometric properties of ice sheet and bed (Schroeder et al., 2014). However the  
998 improvement in radar techniques and the combination with seismic surveys and direct access observations, is our  
999 best chance to improve our observations of subglacial hydrology (Ashmore and Bingham, 2014).

1000 The inventory of subglacial lakes (Wright and Siegert, 2012) is a better constrained and expanding dataset.  
1001 Subglacial lakes can be detected also using satellite surface altimetry (Fricker et al., 2007), providing a way to  
1002 expand the coverage and to confirm dubious cases. However, as noted in Section 5.1., topography must be  
1003 considered when using evidence for subglacial lakes as they can only develop in topographic depressions, and the  
1004 absence of basal water does not imply the bed is frozen if water can drain away.

1005 Subglacial melting can also be detected in englacial stratigraphy (Section 5.3) but the required radar product  
1006 (internal radar reflective horizons) is not often available. “AntArchitecture” is a SCAR (Scientific Committee on

1007 Antarctic Research) Action Group bringing together key datasets on Antarctic internal layering from the principal  
1008 institutions and scientists who have been responsible for acquiring, processing and storing them over the last four  
1009 decades (AntArchitecture Action Group, 2017). As the coverage of Antarctic internal layers becomes widely  
1010 available, its application to infer GHF will increase in popularity.

1011 Finally, and for any of the glaciological methods described above, the glaciological models used to infer GHF  
1012 have to be improved. The current thermal models used to infer GHF can be classified in two larger groups: 1) 1D  
1013 time-dependent high-complexity models, and 2) 2D/3D steady-state low-complexity models. The first category is  
1014 generally used near ice domes or ridges, with low horizontal flow, and where horizontal heat advection can be  
1015 neglected (e.g., Passalacqua, 2017). The latter are used across the whole continent (e.g. Van Liefferinge et al.,  
1016 2018), but ignore the changes in temperature between glacial and interglacial periods despite their strong effect  
1017 on englacial temperatures (Ritz, 1989). The challenge is to develop thermal models with the required level of  
1018 complexity at a continental scale, accommodating the main physical processes. This remains a technical challenge,  
1019 and thermodynamic models remain dependant on GHF estimates.

## 1020 **8. Conclusions**

1021 We present state-of-the-art data and models to estimate geothermal heat flow in Antarctica and highlight the need  
1022 for a detailed continental map. We also discuss current challenges and future directions.

1023 With multiple methodologies and models for Antarctic GHF currently published, the most promising future  
1024 direction for local estimates is borehole-derived estimation of GHF beneath the Antarctic ice sheet from RAID  
1025 bedrock drilling and englacial temperatures from ice boreholes. Ideally, the latter approach will be validated by  
1026 the former to support expansion of the dataset from shallow boreholes (potentially only 600 m deep, or 20 % of  
1027 the total ice sheet thickness).

1028 The ice sheet is most sensitive to variation in GHF within the interior of Antarctica, where heat production from  
1029 sliding at the base of the ice sheet is negligible. However, it is in this region that GHF is hardest to constrain by  
1030 geophysical estimates because of the scarcity of local GHF estimates from down-hole measured temperature  
1031 gradients, geological data, and insight from conjugate margins. It is thus in the interior of Antarctica where  
1032 glaciological approaches are the most applicable. Out of the methods presented, the determination of englacial  
1033 temperatures from long-wavelength microwave emissivity is the most promising, but this data is not currently  
1034 available and requires further validation.

1035 We highlight the potential of regional estimates of GHF from subglacial meltwater inventories. Aside from the  
1036 ever expanding inventory of subglacial lakes we encourage initiatives like “AntArchitecture” that will make radar  
1037 products widely available. Also, we discuss future requirements of thermal models (either 1D or those lacking  
1038 glacial-interglacial variability) to expand the methods beyond domes in the interior of Antarctica.

1039 Geophysical methods remain the most attractive approach to estimate GHF because they are independent of ice  
1040 flow. However, they vary greatly in their estimated magnitude and distribution of GHF. The greatest uncertainty  
1041 in all the geophysical models is uncertainty in the composition and structure of the lithosphere and mantle. We  
1042 recommend ceasing to use the exponential decrease model of crustal heat production. Instead, we suggest using  
1043 geological and geophysical approaches to model the thickness, structure and composition of the crust. We also

1044 recommend the application of a thermal-isostatic approach to provide an independent estimate, and highlight  
1045 regions of anomalous isostatic elevation and probable mantle heterogeneities. The effects of topography must also  
1046 be considered in all GHF models.

1047 Finally, the greatest challenge for Antarctic GHF estimation is the necessity for multidisciplinary science and how  
1048 best to integrate the different methods. Hopefully, this paper provides a first step in communicating the approaches  
1049 and limitations of the different fields across the GHF community. We sincerely recommend the continuation and  
1050 enhancement of the international collaborations within SCAR, building on the work of the GHF sub-group of the  
1051 SERCE research programme (Solid Earth Response and influence on Cryospheric Evolution), and encourage and  
1052 appreciate SCAR's continuing support in this field of research.

### 1053 **Data availability**

1054 The database of GHF point estimates (Fig. 15) is available in the Supplementary Material and from  
1055 <https://github.com/RicardaDziadek/Antarctic-GHF-DB>. The GHF mean and standard deviation maps of the  
1056 geophysical models of continental GHF (Fig. 5f and 5g) are available in the Supplementary Material.

### 1057 **Author contributions**

1058 ABJ and RD conceived the project. ABJ was the lead author for all sections and the specialist in geology and  
1059 geochemistry. RD was a co-author for all sections, compiler of the supplemental GHF database, and the specialist  
1060 in geophysics. CM was a co-author for all sections and the specialist in glaciology.

### 1061 **Competing interests**

1062 The authors declare that they have no conflicts of interest.

### 1063 **Acknowledgements**

1064 The authors thank Brice Van Liefferinge, an anonymous reviewer, and John Goodge for their helpful and thorough  
1065 reviews and comments, which have all improved this final manuscript, Alexander Robinson for his work and  
1066 comments as our handling editor, and the Copernicus team for all their assistance. This research is a contribution  
1067 to the SCAR SERCE scientific research programme, and we thank the discussions and support of this group from  
1068 the TACTical 2018 (Hobart, Australia), POLAR 2018 (Davos, Switzerland), ISAES 2019 (Incheon, Korea), and  
1069 SCAR 2020 Open Science Conference (online) meetings. We particularly thank Jacqueline Halpin (IMAS,  
1070 Hobart) for her comments on the manuscript and her work promoting and developing the Antarctic GHF  
1071 community.

### 1072 **Financial support**

1073 A. Burton-Johnson and C. Martin were funded by the Natural Environment Research Council as part of the British  
1074 Antarctic Survey Polar Science for Planet Earth programme. R. Dziadek was supported by the Deutsche  
1075 Forschungsgemeinschaft (DFG) in the framework of the Priority Program 1158 "Antarctic research with  
1076 comparative investigations in Arctic ice areas" by grant GO 724/14-1. Additional funds were contributed by the  
1077 AWI Research Program PACES-II Workpackage 3.2.

1078 **Review statement**

1079 This paper was reviewed by Brice Van Liefvering and an anonymous reviewer. Alexander Robinson was the  
1080 handling editor. John Goodge provided an additional short comment in the interactive discussion.

1081 **9. References**

- 1082 Aboud, E., Salem, A. and Mekkawi, M.: Curie depth map for Sinai Peninsula, Egypt deduced from the analysis  
1083 of magnetic data, *Tectonophysics*, 506(1–4), 46–54, 2011.
- 1084 Aitken, A. R. A., Betts, P. G., Young, D. A., Blankenship, D. D., Roberts, J. L. and Siegert, M. J.: The Australo-  
1085 Antarctic Columbia to Gondwana transition, *Gondwana Research*, 29(1), 136–152, 2016.
- 1086 Alessio, K. L., Hand, M., Kelsey, D. E., Williams, M. A., Morrissey, L. J. and Barovich, K.: Conservation of deep  
1087 crustal heat production, *Geology*, 46(4), 335–338, 2018.
- 1088 Amante, C. and Eakins, B. W.: ETOPO1 Arc-Minute Global Relief Model: Procedures, Data Sources and  
1089 Analysis, National Oceanic and Atmospheric Administration Technical Memorandum NESDIS NGDC-24., 2009.
- 1090 An, M., Wiens, D. A., Zhao, Y., Feng, M., Nyblade, A. A., Kanao, M., Li, Y., Maggi, A. and L ev eque, J.-J.: S-  
1091-velocity model and inferred Moho topography beneath the Antarctic Plate from Rayleigh waves, *Journal of*  
1092 *Geophysical Research: Solid Earth*, 120(1), 359–383, 2015a.
- 1093 An, M., Wiens, D. A., Zhao, Y., Feng, M., Nyblade, A., Kanao, M., Li, Y., Maggi, A. and L ev eque, J.-J.:  
1094 Temperature, lithosphere-asthenosphere boundary, and heat flux beneath the Antarctic Plate inferred from seismic  
1095 velocities, *Journal of Geophysical Research: Solid Earth*, 120(12), 8720–8742, 2015b.
- 1096 Andr es, J., Marz an, I., Ayarza, P., Mart ı, D., Palomeras, I., Torn e, M., Campbell, S. and Carbonell, R.: Curie point  
1097 depth of the Iberian Peninsula and surrounding margins. A thermal and tectonic perspective of its evolution,  
1098 *Journal of Geophysical Research: Solid Earth*, 123(3), 2049–2068, 2018.
- 1099 AntArchitecture Action Group: AntArchitecture: Archiving and interrogating Antarctica’s internal structure from  
1100 radar sounding. Final Report, in Workshop to establish scientific goals, working practices and funding routes.  
1101 University of Edinburgh, UK, University of Edinburgh, UK. [online] Available from:  
1102 <https://www.scar.org/library/science-4/geosciences/antarchitecture/5240-antarchitecture-workshop-2017/file>,  
1103 2017.
- 1104 Arnaiz-Rodr ıguez, M. S. and Orihuela, N.: Curie point depth in Venezuela and the Eastern Caribbean,  
1105 *Tectonophysics*, 590, 38–51, 2013.
- 1106 Artemieva, I.: *Lithosphere: an interdisciplinary approach*, Cambridge University Press, Cambridge, UK., 2011.
- 1107 Artemieva, I. M. and Mooney, W. D.: Thermal thickness and evolution of Precambrian lithosphere: A global  
1108 study, *Journal of Geophysical Research: Solid Earth*, 106(B8), 16387–16414, 2001.
- 1109 Ashmore, D. W. and Bingham, R. G.: Antarctic subglacial hydrology: current knowledge and future challenges,  
1110 *Antarctic Science*, 26(6), 758–773, 2014.
- 1111 Bansal, A. R., Gabriel, G., Dimri, V. P. and Krawczyk, C. M.: Estimation of depth to the bottom of magnetic  
1112 sources by a modified centroid method for fractal distribution of sources: An application to aeromagnetic data in  
1113 Germany, *Geophysics*, 76(3), L11–L22, 2011.
- 1114 Bansal, A. R., Anand, S. P., Rajaram, M., Rao, V. K. and Dimri, V. P.: Depth to the bottom of magnetic sources  
1115 (DBMS) from aeromagnetic data of Central India using modified centroid method for fractal distribution of  
1116 sources, *Tectonophysics*, 603, 155–161, 2013.
- 1117 Barletta, V. R., Bevis, M., Smith, B. E., Wilson, T., Brown, A., Bordoni, A., Willis, M., Khan, S. A., Rovira-  
1118 Navarro, M. and Dalziel, I.: Observed rapid bedrock uplift in Amundsen Sea Embayment promotes ice-sheet  
1119 stability, *Science*, 360(6395), 1335–1339, 2018.

- 1120 Baron Fourier, J. B. J.: *Théorie analytique de la chaleur*, Chez Firmin Didot, père et fils, Paris., 1822.
- 1121 Barrett, B. E., Nicholls, K. W., Murray, T., Smith, A. M. and Vaughan, D. G.: Rapid recent warming on Rutford  
1122 Ice Stream, West Antarctica, from borehole thermometry, *Geophysical Research Letters*, 36(2), 2009.
- 1123 Bea, F.: The sources of energy for crustal melting and the geochemistry of heat-producing elements, *Lithos*, 153,  
1124 278–291, doi:10.1016/j.lithos.2012.01.017, 2012.
- 1125 Bea, F. and Montero, P.: Behavior of accessory phases and redistribution of Zr, REE, Y, Th, and U during  
1126 metamorphism and partial melting of metapelites in the lower crust: an example from the Kinzigite Formation of  
1127 Ivrea-Verbanò, NW Italy, *Geochimica et Cosmochimica Acta*, 63(7), 1133–1153, 1999.
- 1128 Beamish, D. and Busby, J.: The Cornubian geothermal province: heat production and flow in SW England:  
1129 estimates from boreholes and airborne gamma-ray measurements, *Geothermal Energy*, 4(1), 4, 2016.
- 1130 Beardsmore, G. R. and Cull, J. P.: *Crustal heat flow: a guide to measurement and modelling*, Cambridge  
1131 University Press, Cambridge, UK., 2001.
- 1132 Begeman, C. B., Tulaczyk, S. M. and Fisher, A. T.: Spatially variable geothermal heat flux in West Antarctica:  
1133 evidence and implications, *Geophysical Research Letters*, 44(19), 9823–9832, 2017.
- 1134 Berg, J. H., Moscati, R. J. and Herz, D. L.: A petrologic geotherm from a continental rift in Antarctica, *Earth and  
1135 Planetary Science Letters*, 93(1), 98–108, 1989.
- 1136 Bhattacharyya, B. K. and Leu, L.-K.: Analysis of magnetic anomalies over Yellowstone National Park: mapping  
1137 of Curie point isothermal surface for geothermal reconnaissance, *Journal of Geophysical Research*, 80(32), 4461–  
1138 4465, 1975.
- 1139 Blakely, R. J.: *Potential theory in gravity and magnetic applications*, Cambridge university press, Cambridge,  
1140 UK., 1996.
- 1141 Blakely, R. J., Brocher, T. M. and Wells, R. E.: Subduction-zone magnetic anomalies and implications for  
1142 hydrated forearc mantle, *Geology*, 33(6), 445–448, 2005.
- 1143 Boden, D. R.: *Geology and Heat Architecture of the Earth's Interior*, in *Geologic Fundamentals of Geothermal  
1144 Energy*, Routledge., 2016.
- 1145 Bodorkos, S., Sandiford, M., Minty, B. R. and Blewett, R. S.: A high-resolution, calibrated airborne radiometric  
1146 dataset applied to the estimation of crustal heat production in the Archaean northern Pilbara Craton, Western  
1147 Australia, *Precambrian Research*, 128(1–2), 57–82, 2004.
- 1148 Bucher, G. J.: Heat flow and radioactivity studies in the Ross Island-Dry Valley area, Antarctica and their tectonic  
1149 implications., PhD Thesis, University of Wyoming, Wyoming, USA., 1980.
- 1150 Bucker, C., Jarrard, R. D. and Wonik, T.: Downhole temperature, radiogenic heat production, and heat flow from  
1151 the CRP-3 drillhole, Victoria Land Basin, Antarctica, *Terra Antarctica*, 8(3), 151–160, 2001.
- 1152 Bullard, E. C.: The disturbance of the temperature gradient in the earth's crust by inequalities of height,  
1153 *Geophysical Supplements to the Monthly Notices of the Royal Astronomical Society*, 4(5), 360–362, 1938.
- 1154 Bullard, E. C.: The time taken for a borehole to attain temperature equilibrium, *Monthly Notices of the Royal  
1155 Astronomical Society, Geophysics Supplement*, 5, 127–130, 1947.
- 1156 Burton-Johnson, A., Halpin, J. A., Whittaker, J. M., Graham, F. S. and Watson, S. J.: A new heat flux model for  
1157 the Antarctic Peninsula incorporating spatially variable upper crustal radiogenic heat production, *Geophysical  
1158 Research Letters*, 44(11), 5436–5446, doi:10.1002/2017GL073596, 2017.

- 1159 Burton-Johnson, A., Dziadek, R. and Shen, W.: Report of the Geothermal Heat Flux Side Meeting at XIII ISAES,  
1160 2019, Incheon, Republic of Korea. [online] Available from: <https://www.scar.org/scar-library/search/science-4/research-programmes/serce/5334-ghf-meeting-report-2019/file>, 2019.
- 1162 Burton-Johnson, A., Dziadek, R., Martin, C., Halpin, J. A., Whitehouse, P. L., Ebbing, J., Martos, Y. M., Martin,  
1163 A. P., Schroeder, D. M., Shen, W., Ritz, C., Goodge, J. W., Van Liefferinge, B., Pattyn, F., Reading, A. M.,  
1164 Ferraccioli, F. and The SERCE Geothermal Heat Flow Sub-Group: Antarctic Geothermal Heat Flow: Future  
1165 research directions, SCAR-SERCE White Paper [online] Available from: <https://www.scar.org/scar-library/search/science-4/research-programmes/serce/5454-scar-serce-white-paper-on-antarctic-geothermal-heat-flow/>, 2020.
- 1168 Carlson, R. W., Pearson, D. G. and James, D. E.: Physical, chemical and chronological characteristics of  
1169 continental mantle, *Reviews in Geophysics*, 43, RG1001, doi:10.1029/2004RG000156, 2005.
- 1170 Carslaw, H. S. and Jaeger, J. C.: *Conduction of heat in solids*, Oxford: Clarendon Press, 1959, 2nd ed., 1959.
- 1171 Carson, C. J. and Pittard, M.: *A Reconnaissance Crustal Heat Production Assessment of the Australian Antarctic  
1172 Territory (AAT)*, Geoscience Australia, Canberra, Australia., 2012.
- 1173 Carson, C. J., McLaren, S., Roberts, J. L., Boger, S. D. and Blankenship, D. D.: Hot rocks in a cold place: high  
1174 sub-glacial heat flow in East Antarctica, *Journal of the Geological Society*, 171(1), 9–12, 2014.
- 1175 Carter, S. P., Blankenship, D. D., Young, D. A. and Holt, J. W.: Using radar-sounding data to identify the  
1176 distribution and sources of subglacial water: application to Dome C, East Antarctica, *Journal of Glaciology*,  
1177 55(194), 1025–1040, 2009.
- 1178 Chen, B., Haeger, C., Kaban, M. K. and Petrunin, A. G.: Variations of the effective elastic thickness reveal tectonic  
1179 fragmentation of the Antarctic lithosphere, *Tectonophysics*, 746, 412–424, 2018.
- 1180 Clauser, C., Giese, P., Huenges, E., Kohl, T., Lehmann, H., Rybach, L., Šafanda, J., Wilhelm, H., Windloff, K.  
1181 and Zoth, G.: The thermal regime of the crystalline continental crust: implications from the KTB, *Journal of  
1182 Geophysical Research: Solid Earth*, 102(B8), 18417–18441, 1997.
- 1183 Clow, G. D., Cuffey, K. M. and Waddington, E. D.: High heat-flow beneath the central portion of the West  
1184 Antarctic Ice Sheet, in *AGU Fall Meeting Abstracts.*, 2012.
- 1185 Courtney, R. C. and White, R. S.: Anomalous heat flow and geoid across the Cape Verde Rise: evidence for  
1186 dynamic support from a thermal plume in the mantle, *Geophysical Journal International*, 87(3), 815–867, 1986.
- 1187 Cuffey, K. M. and Paterson, W. S. B.: *The physics of glaciers*, 4th Edition., Elsevier, Oxford, UK., 2010.
- 1188 Cuffey, K. M., Clow, G. D., Alley, R. B., Stuiver, M., Waddington, E. D. and Saltus, R. W.: Large arctic  
1189 temperature change at the Wisconsin-Holocene glacial transition, *Science*, 270(5235), 455–458, 1995.
- 1190 Daczko, N. R., Halpin, J. A., Fitzsimons, I. C. and Whittaker, J. M.: A cryptic Gondwana-forming orogen located  
1191 in Antarctica, *Scientific reports*, 8(1), 8371, 2018.
- 1192 Dahl-Jensen, D., Morgan, V. I. and Elcheikh, A.: Monte Carlo inverse modelling of the Law Dome (Antarctica)  
1193 temperature profile, *Annals of Glaciology*, 29, 145–150, 1999.
- 1194 Dalby, C. J., Shail, R. K., Batchelor, A., Cotton, L., Gutmanis, J., Rollinson, G. K., Wall, F. and Hickey, J.: Deep  
1195 geothermal energy from the Cornubian Batholith: preliminary lithological and heat flow insights from the United  
1196 Downs Deep Geothermal Power Project, Plymouth, UK., 2020.
- 1197 Davis, E. E., Villinger, H., MacDonald, R. D., Meldrum, R. D. and Grigel, J.: A robust rapid-response probe for  
1198 measuring bottom-hole temperatures in deep-ocean boreholes, *Marine Geophysical Researches*, 19(3), 267–281,  
1199 1997.

- 1200 Decker, E. R.: Preliminary geothermal studies of the Dry Valley Drilling Project holes at McMurdo Station, Lake  
1201 Vanda, Lake Vida, and New Harbor, Antarctica, *Bulletin-Dry Valley Drilling Project (DVDP)*, 4, 22–23, 1974.
- 1202 Decker, E. R. and Bucher, G. J.: Geothermal studies in the Ross Island-Dry Valley region, *Antarct Geosci*, 4, 887–  
1203 894, 1982.
- 1204 Decker, E. R., Baker, K. H. and Harris, H.: Geothermal studies in the Dry Valleys and on Ross Island, *Antarctic  
1205 Journal*, 10(4), 176, 1975.
- 1206 Dymant, J. and Arkani-Hamed, J.: Equivalent source magnetic dipoles revisited, *Geophysical Research Letters*,  
1207 25(11), 2003–2006, 1998.
- 1208 Dziadek, R., Gohl, K., Diehl, A. and Kaul, N.: Geothermal heat flux in the Amundsen Sea sector of West  
1209 Antarctica: New insights from temperature measurements, depth to the bottom of the magnetic source estimation,  
1210 and thermal modeling, *Geochemistry, Geophysics, Geosystems*, 18(7), 2657–2672, 2017.
- 1211 Dziadek, R., Gohl, K. and Kaul, N.: Elevated geothermal surface heat flow in the Amundsen Sea Embayment,  
1212 West Antarctica, *Earth and Planetary Science Letters*, 506, 530–539, 2019.
- 1213 Ebbing, J., Lundin, E., Olesen, O. and Hansen, E. K.: The mid-Norwegian margin: a discussion of crustal  
1214 lineaments, mafic intrusions, and remnants of the Caledonian root by 3D density modelling and structural  
1215 interpretation, *Journal of the Geological Society*, 163(1), 47–59, 2006.
- 1216 Ebbing, J., Gernigon, L., Pascal, C., Olesen, O. and Osmundsen, P. T.: A discussion of structural and thermal  
1217 control of magnetic anomalies on the mid-Norwegian margin, *Geophysical Prospecting*, 57(4), 665–681, 2009.
- 1218 Elbeze, A. C.: On the existence of another source of heat production for the earth and planets, and its connection  
1219 with gravitomagnetism, *SpringerPlus*, 2(1), 1–13, doi:10.1186/2193-1801-2-513, 2013.
- 1220 Engelhardt, H.: Ice temperature and high geothermal flux at Siple Dome, West Antarctica, from borehole  
1221 measurements, *Journal of Glaciology*, 50(169), 251–256, 2004.
- 1222 Fahnestock, M., Abdalati, W., Joughin, I., Brozena, J. and Gogineni, P.: High geothermal heat flow, basal melt,  
1223 and the origin of rapid ice flow in central Greenland, *Science*, 294(5550), 2338–2342, 2001.
- 1224 Ferraccioli, F., Finn, C. A., Jordan, T. A., Bell, R. E., Anderson, L. M. and Damaske, D.: East Antarctic rifting  
1225 triggers uplift of the Gamburtsev Mountains, *Nature*, 479(7373), 388–392, 2011.
- 1226 Ferré, E. C., Friedman, S. A., Martín-Hernández, F., Feinberg, J. M., Conder, J. A. and Ionov, D. A.: The  
1227 magnetism of mantle xenoliths and potential implications for sub-Moho magnetic sources, *Geophysical Research  
1228 Letters*, 40(1), 105–110, 2013.
- 1229 Fischer, H., Severinghaus, J., Brook, E., Wolff, E., Albert, M., Alemany, O., Arthern, R., Bentley, C.,  
1230 Blankenship, D., Chappellaz, J. and others: Where to find 1.5 million yr old ice for the IPICS" Oldest-Ice" ice  
1231 core, *Climate of the Past*, 9(6), 2489–2505, 2013.
- 1232 Fisher, A. T. and Harris, R. N.: Using seafloor heat flow as a tracer to map subseafloor fluid flow in the ocean  
1233 crust, *Geofluids*, 10(1–2), 142–160, 2010.
- 1234 Fisher, A. T., Mankoff, K. D., Tulaczyk, S. M., Tyler, S. W., Foley, N. and others: High geothermal heat flux  
1235 measured below the West Antarctic Ice Sheet, *Science advances*, 1(6), e1500093, 2015.
- 1236 Flowerdew, M. J., Tyrrell, S., Boger, S. D., Fitzsimons, I. C. W., Harley, S. L., Mikhalsky, E. V. and Vaughan,  
1237 A. P. M.: Pb isotopic domains from the Indian Ocean sector of Antarctica: implications for past Antarctica–India  
1238 connections, *Geological Society, London, Special Publications*, 383(1), 59–72, 2013.
- 1239 Foster, T. D.: Temperature and salinity fields under the Ross Ice Shelf, *Antarctic Journal [of the United States]*,  
1240 13, 81–82, 1978.

- 1241 Fox Maule, C., Purucker, M. E., Olsen, N. and Mosegaard, K.: Heat flux anomalies in Antarctica revealed by  
1242 satellite magnetic data, *Science*, 309(5733), 464–467, 2005.
- 1243 Fricker, H. A., Scambos, T., Bindschadler, R. and Padman, L.: An active subglacial water system in West  
1244 Antarctica mapped from space, *Science*, 315(5818), 1544–1548, 2007.
- 1245 Frost, B. R. and Shive, P. N.: Magnetic mineralogy of the lower continental-crust, *Journal of Geophysical  
1246 Research-Solid Earth and Planets*, 91(B6), 6513–6521, 1986.
- 1247 Fudge, T. J., Biyani, S., Clemens-Sewall, D. and Hawley, B.: Constraining geothermal flux at coastal domes of  
1248 the Ross Ice Sheet, Antarctica, *Geophysical Research Letters*, 46(22), 13090–13098, 2019.
- 1249 Gard, M., Hasterok, D. and Halpin, J. A.: Global whole-rock geochemical database compilation, *Earth System  
1250 Science Data*, 11(4), 1553–1566, doi:<https://doi.org/10.5194/essd-2019-50>, 2019.
- 1251 Godey, S., Deschamps, F., Trampert, J. and Snieder, R.: Thermal and compositional anomalies beneath the North  
1252 American continent, *Journal of Geophysical Research: Solid Earth*, 109(B1), 2004.
- 1253 Goelzer, H., Robinson, A., Seroussi, H. and Van De Wal, R. S.: Recent progress in Greenland ice sheet modelling,  
1254 *Current climate change reports*, 3(4), 291–302, 2017.
- 1255 Gohl, K., Wellner, J. S., Klaus, A. and Expedition 379 Scientists: Expedition 379 Preliminary Report: Amundsen  
1256 Sea West Antarctic Ice Sheet History, *International Ocean Discovery Program*, 379,  
1257 doi:<https://doi.org/10.14379/iodp.pr.379.2019>, 2019.
- 1258 Golynsky, A., Chiappini, M., Damaske, D., Ferraccioli, F., Finn, C. A., Ishihara, T., Kim, H. R., Kovacs, L.,  
1259 Masolov, V. N., Morris, P. and others: ADMAP—a digital magnetic anomaly map of the Antarctic, in *Antarctica*,  
1260 pp. 109–116, Springer., 2006.
- 1261 Goodge, J. W.: Crustal heat production and estimate of terrestrial heat flow in central East Antarctica, with  
1262 implications for thermal input to the East Antarctic ice sheet., *Cryosphere*, 12, 491–504,  
1263 doi:<https://doi.org/10.5194/tc-12-491-2018>, 2018.
- 1264 Goodge, J. W. and Severinghaus, J. P.: Rapid Access Ice Drill: a new tool for exploration of the deep Antarctic  
1265 ice sheets and subglacial geology, *Journal of Glaciology*, 62(236), 1049–1064, 2016.
- 1266 Gow, A. J., Ueda, H. T. and Garfield, D. E.: Antarctic ice sheet: preliminary results of first core hole to bedrock,  
1267 *Science*, 161(3845), 1011–1013, 1968.
- 1268 Granot, R. and Dymant, J.: Late Cenozoic unification of East and West Antarctica, *Nature communications*, 9(1),  
1269 3189, 2018.
- 1270 Grauch, V. J. S.: Limitations on digital filtering of the DNAG magnetic data set for the conterminous US,  
1271 *Geophysics*, 58(9), 1281–1296, 1993.
- 1272 Greve, R. and Hutter, K.: Polythermal three-dimensional modelling of the Greenland ice sheet with varied  
1273 geothermal heat flux, *Annals of Glaciology*, 21(1), 8–12, 1995.
- 1274 Guimarães, S. N. P., Hamza, V. M. and Ravat, D.: Curie depths using combined analysis of centroid and matched  
1275 filtering methods in inferring thermomagnetic characteristics of Central Brazil, in 13th International Congress of  
1276 the Brazilian Geophysical Society & EXPOGEF, Rio de Janeiro, Brazil, 26–29 August 2013, pp. 1853–1858,  
1277 Society of Exploration Geophysicists and Brazilian Geophysical Society., 2013.
- 1278 Gutenberg, B.: 6. Temperature and Thermal Processes in the Earth, in *International Geophysics*, vol. 1, edited by  
1279 B. Gutenberg, pp. 121–148, Academic Press Inc., New York., 1959.
- 1280 Haggerty, S. E.: Mineralogical constraints on Curie isotherms in deep crustal magnetic anomalies, *Geophysical  
1281 Research Letters*, 5(2), 105–108, 1978.

- 1282 Halpin, J. A. and Reading, A. M.: Report on Taking the Temperature of the Antarctic Continent (TACTical)  
1283 Workshop 21-23 March 2018, Hobart, Tasmania, Australia, Hobart, Australia., 2018.
- 1284 Halpin, J. A., Whittaker, J. M., Gard, M., Hasterok, D., Burton-Johnson, A., Staal, T., Maritati, A., Reading, A.  
1285 M., McLaren, S., Hand, M. and Raimondo, T.: Heterogenous Antarctic crustal heat production, Incheon, Republic  
1286 of Korea., 2019.
- 1287 Hasterok, D. and Chapman, D. S.: Continental thermal isostasy: 1. Methods and sensitivity, *Journal of*  
1288 *Geophysical Research: Solid Earth*, 112(B6), 2007a.
- 1289 Hasterok, D. and Chapman, D. S.: Continental thermal isostasy: 2. Application to North America, *Journal of*  
1290 *Geophysical Research: Solid Earth*, 112(B6), 2007b.
- 1291 Hasterok, D. and Chapman, D. S.: Heat production and geotherms for the continental lithosphere, *Earth and*  
1292 *Planetary Science Letters*, 307(1–2), 59–70, doi:10.1016/j.epsl.2011.04.034, 2011.
- 1293 Hasterok, D. and Gard, M.: Utilizing thermal isostasy to estimate sub-lithospheric heat flow and anomalous crustal  
1294 radioactivity, *Earth and Planetary Science Letters*, 450, 197–207, 2016.
- 1295 Hasterok, D., Gard, M., Halpin, J. A., Hand, M. P., Pollett, A., McLaren, S., Raimondo, T., Willcocks, S. and  
1296 Linke, M.: Constraining Geothermal Heat Flux Beneath Ice Sheets Using Thermal Isostasy, in *AGU Fall Meeting*  
1297 *2019, AGU.*, 2019.
- 1298 Heesemann, M., Villinger, H., Fisher, A. T., Tréhu, A. M. and White, S.: Data report: testing and deployment of  
1299 the new APCT-3 tool to determine in situ temperatures while piston coring, in *Proceedings of the Integrated Ocean*  
1300 *Drilling Program*, 311, edited by M. Riedel, T. Collett, M. Malone, and the Expedition 311 Scientists, *Integrated*  
1301 *Ocean Drilling Program Management International, Inc.*, Washington, DC., 2006.
- 1302 Hillenbrand, C.-D., Smith, J. A., Hodell, D. A., Greaves, M., Poole, C. R., Kender, S., Williams, M., Andersen,  
1303 T. J., Jernas, P. E. and Elderfield, H.: West Antarctic Ice Sheet retreat driven by Holocene warm water incursions,  
1304 *Nature*, 547(7661), 43, 2017.
- 1305 Hindmarsh, R. C. and Ritz, C. M.: How deep do you need to drill through ice to measure the geothermal heat  
1306 flux?, in *EGU General Assembly Conference Abstracts*, vol. 14, p. 8629., 2012.
- 1307 Hondoh, T., Shoji, H., Watanabe, O., Salamatina, A. N. and Lipenkova, V. Y.: Depth–age and temperature  
1308 prediction at Dome Fuji station, East Antarctica, *Annals of Glaciology*, 35, 384–390, 2002.
- 1309 Huang, Y., Chubakov, V., Mantovani, F., Rudnick, R. L. and McDonough, W. F.: A reference Earth model for  
1310 the heat-producing elements and associated geoneutrino flux, *Geochemistry, Geophysics, Geosystems*, 14(6),  
1311 2003–2029, 2013.
- 1312 Hughes, T.: Modeling ice sheets from the bottom up, *Quaternary Science Reviews*, 28(19–20), 1831–1849, 2009.
- 1313 Hyndman, R. D., Langseth, M. G. and Von Herzen, R. P.: Deep Sea Drilling Project geothermal measurements:  
1314 a review, *Reviews of geophysics*, 25(8), 1563–1582, 1987.
- 1315 Hyvönen, E., Turunen, P., Vanhanen, E., Arkimaa, H. and Sutinen, R.: Airborne gamma-ray surveys in Finland,  
1316 *Aerogeophysics in Finland*, 2004, 1972.
- 1317 Jaeger, J. C.: Numerical values for the temperature in radial heat flow, *Journal of Mathematics and Physics*, 34(1–  
1318 4), 316–321, 1956.
- 1319 Jaeger, J. C.: The effect of the drilling fluid on temperatures measured in bore holes, *Journal of Geophysical*  
1320 *Research*, 66(2), 563–569, 1961.
- 1321 Jaeger, J. C.: Application of the theory of heat conduction to geothermal measurements, *Terrestrial heat flow*, 8,  
1322 7–23, 1965.

- 1323 James, D. W.: The thermal diffusivity of ice and water between- 40 and+ 60° C, *Journal of Materials Science*,  
1324 3(5), 540–543, 1968.
- 1325 Jezek, K. C., Johnson, J. T., Drinkwater, M. R., Macelloni, G., Tsang, L., Aksoy, M. and Durand, M.: Radiometric  
1326 approach for estimating relative changes in intraglacier average temperature, *IEEE Transactions on Geoscience  
1327 and Remote Sensing*, 53(1), 134–143, 2014.
- 1328 Jordan, T., Martin, C., Ferraccioli, F., Matsuoka, K., Corr, H., Forsberg, R., Olesen, A. and Siegert, M. J.: Newly  
1329 discovered geothermal anomaly at South Pole ice divide; origins and implications, in *Geophysical Research  
1330 Abstracts*, vol. 20, p. 15511., 2018.
- 1331 Jordan, T. A., Riley, T. R. and Siddoway, C. S.: The geological history and evolution of West Antarctica, *Nature  
1332 Reviews Earth & Environment*, 1, 117–133, 2020.
- 1333 Kawakatsu, H. and Watada, S.: Seismic evidence for deep-water transportation in the mantle, *Science*, 316(5830),  
1334 1468–1471, 2007.
- 1335 Kerr, Y. H., Waldteufel, P., Wigneron, J.-P., Delwart, S., Cabot, F., Boutin, J., Escorihuela, M.-J., Font, J., Reul,  
1336 N. and Gruhier, C.: The SMOS mission: New tool for monitoring key elements of the global water cycle,  
1337 *Proceedings of the IEEE*, 98(5), 666–687, 2010.
- 1338 Kingslake, J., Scherer, R. P., Albrecht, T., Coenen, J., Powell, R. D., Reese, R., Stansell, N. D., Tulaczyk, S.,  
1339 Wearing, M. G. and Whitehouse, P. L.: Extensive retreat and re-advance of the West Antarctic Ice Sheet during  
1340 the Holocene, *Nature*, 558(7710), 430–434, 2018.
- 1341 Korenaga, J.: Earth’s heat budget: Clairvoyant geoneutrinos, *Nature Geoscience*, 4(9), 581, 2011.
- 1342 Kuchar, J. and Milne, G. A.: The influence of viscosity structure in the lithosphere on predictions from models of  
1343 glacial isostatic adjustment, *Journal of Geodynamics*, 86, 1–9, 2015.
- 1344 Lachenbruch, A. H.: Preliminary geothermal model of the Sierra Nevada, *Journal of Geophysical Research*,  
1345 73(22), 6977–6989, 1968.
- 1346 Lachenbruch, A. H.: Crustal temperature and heat production: Implications of the linear heat-flow relation, *Journal  
1347 of Geophysical Research*, 75(17), 3291–3300, 1970.
- 1348 Lachenbruch, A. H. and Brewer, M. C.: Dissipation of the temperature effect of drilling a well in Arctic Alaska,  
1349 *United States Geological Survey Bulletin*, 1083–C, 73–109, 1959.
- 1350 Langel, R. A. and Hinze, W. J.: *The magnetic field of the Earth’s lithosphere: The satellite perspective*, Cambridge  
1351 University Press, Cambridge, UK., 1998.
- 1352 Larour, E., Morlighem, M., Seroussi, H., Schiermeier, J. and Rignot, E.: Ice flow sensitivity to geothermal heat  
1353 flux of Pine Island Glacier, Antarctica, *Journal of Geophysical Research: Earth Surface*, 117(F4), 2012.
- 1354 Leat, P. T., Jordan, T. A., Flowerdew, M. J., Riley, T. R., Ferraccioli, F. and Whitehouse, M. J.: Jurassic high heat  
1355 production granites associated with the Weddell Sea rift system, Antarctica, *Tectonophysics*, 722, 249–264, 2018.
- 1356 Lees, C. H.: On the shapes of the isogeotherms under mountain ranges in radio-active districts, *Proceedings of the  
1357 Royal Society of London. Series A, Containing Papers of a Mathematical and Physical Character*, 83(563), 339–  
1358 346, 1910.
- 1359 Li, C.-F., Lu, Y. and Wang, J.: A global reference model of Curie-point depths based on EMAG2, *Scientific  
1360 reports*, 7, 45129, 2017.
- 1361 Llubes, M., Lanseau, C. and Rémy, F.: Relations between basal condition, subglacial hydrological networks and  
1362 geothermal flux in Antarctica, *Earth and Planetary Science Letters*, 241(3), 655–662, 2006.
- 1363 Lowrie, W.: *Fundamentals of geophysics*, 2nd ed., Cambridge University Press, Cambridge., 2007.

- 1364 Lucazeau, F.: Analysis and mapping of an updated terrestrial heat flow dataset, *Geochemistry, Geophysics, Geosystems*, 20(8), 4001–4024, 2019.
- 1366 Macelloni, G., Leduc-Leballeur, M., Brogioni, M., Ritz, C. and Picard, G.: Analyzing and modeling the SMOS spatial variations in the East Antarctic Plateau, *Remote sensing of environment*, 180, 193–204, 2016.
- 1368 Macelloni, G., Leduc-Leballeur, M., Montomoli, F., Brogioni, M., Ritz, C. and Picard, G.: On the retrieval of internal temperature of Antarctica Ice Sheet by using SMOS observations, *Remote Sensing of Environment*, 233, 111405, 2019.
- 1371 Mareschal, J. C. and Jaupart, C.: Radiogenic heat production, thermal regime and evolution of continental crust, *Tectonophysics*, 609, 524–534, doi:10.1016/j.tecto.2012.12.001, 2013.
- 1373 Martin, A. P. and van der Wal, W., Eds.: *The Antarctic Mantle*, The Geological Society, London, UK., in prep.
- 1374 Martin, A. P., Cooper, A. F. and Price, R. C.: Increased mantle heat flow with on-going rifting of the West Antarctic rift system inferred from characterisation of plagioclase peridotite in the shallow Antarctic mantle, *Lithos*, 190, 173–190, 2014.
- 1377 Martos, Y. M., Catalán, M., Jordan, T. A., Golynsky, A., Golynsky, D., Eagles, G. and Vaughan, D. G.: Heat flux distribution of Antarctica unveiled, *Geophysical Research Letters*, 44(22), 11–417, 2017.
- 1379 Martos, Y. M., Jordan, T. A., Catalán, M., Jordan, T. M., Bamber, J. L. and Vaughan, D. G.: Geothermal heat flux reveals the Iceland hotspot track underneath Greenland, *Geophysical Research Letters*, 45(16), 8214–8222, 2018.
- 1381 Maus, S.: Magnetic field model MF7. Retrieved August 28, 2018, from [www.geomag.us/models/MF7.html](http://www.geomag.us/models/MF7.html), 2010.
- 1383 Mayhew, M. A.: Inversion of satellite magnetic anomaly data, *Journal of Geophysics*, 45(1), 119–128, 1979.
- 1384 McDonough, W. F. and Sun, S. s.: The composition of the Earth, *Chemical Geology*, 120(3–4), 223–253, doi:10.1016/0009-2541(94)00140-4, 1995.
- 1386 McKay, R., De Santis, L., Kulhanek, D. K. and Expedition 374 Scientists: International Ocean Discovery Program Expedition 374 Preliminary Report: Ross Sea West Antarctic Ice Sheet History, International Ocean Discovery Program, 374, doi:<https://doi.org/10.14379/iodp.pr.374.2018>, 2018.
- 1389 McKenzie, D., Jackson, J. and Priestley, K.: Thermal structure of oceanic and continental lithosphere, *Earth and Planetary Science Letters*, 233(3–4), 337–349, 2005.
- 1391 Morgan, J. P., Rüpke, L. H. and White, W. M.: The Current Energetics of Earth’s Interior: A Gravitational Energy Perspective, *Frontiers in Earth Science*, 4(May), 1–28, doi:10.3389/feart.2016.00046, 2016.
- 1393 Morin, R. H., Williams, T., Henrys, S. A., Magens, D., Niessen, F. and Hansaraj, D.: Heat flow and hydrologic characteristics at the AND-1B borehole, ANDRILL McMurdo Ice Shelf Project, Antarctica, *Geosphere*, 6(4), 370–378, 2010.
- 1396 Mulder, J. A., Halpin, J. A., Daczko, N. R., Orth, K., Meffre, S., Thompson, J. M. and Morrissey, L. J.: A Multiproxy provenance approach to uncovering the assembly of East Gondwana in Antarctica, *Geology*, 47(7), 645–649, 2019.
- 1399 Müller, C., Usbeck, R. and Miesner, F.: Temperatures in shallow marine sediments: Influence of thermal properties, seasonal forcing, and man-made heat sources, *Applied Thermal Engineering*, 108, 20–29, 2016.
- 1401 Mulvaney, R., Abram, N. J., Hindmarsh, R. C., Arrowsmith, C., Fleet, L., Triest, J., Sime, L. C., Alemany, O. and Foord, S.: Recent Antarctic Peninsula warming relative to Holocene climate and ice-shelf history, *Nature*, 489(7414), 141–144, 2012.

- 1404 Mulvaney, R., Martin, C., Massam, A., Rix, J. and Ritz, C.: Estimating geothermal heat flux from ice sheet  
1405 borehole temperature measurements, in XIII International Symposium on Antarctic Earth Sciences, Incheon,  
1406 Republic of Korea., 2019.
- 1407 Nicholls, K. W. and Paren, J. G.: Extending the Antarctic meteorological record using ice-sheet temperature  
1408 profiles, *Journal of climate*, 6(1), 141–150, 1993.
- 1409 Obande, G. E., Lawal, K. M. and Ahmed, L. A.: Spectral analysis of aeromagnetic data for geothermal  
1410 investigation of Wikki Warm Spring, north-east Nigeria, *Geothermics*, 50, 85–90, 2014.
- 1411 Okubo, Y., Graf, R. J., Hansen, R. O., Ogawa, K. and Tsu, H.: Curie point depths of the island of Kyushu and  
1412 surrounding areas, Japan, *Geophysics*, 50(3), 481–494, 1985.
- 1413 Olesen, O., Balling, N., Barrère, C., Breiner, N., Davidsen, B., Ebbing, J., Elvebakk, H., Gernigon, L., Koziel, J.,  
1414 Lutro, O. and others: KONTIKI final report, continental crust and heat generation in 3D, NGU Report, 42, 2007.
- 1415 Pappa, F., Ebbing, J., Ferraccioli, F. and van der Wal, W.: Modeling satellite gravity gradient data to derive  
1416 density, temperature, and viscosity structure of the Antarctic lithosphere, *Journal of Geophysical Research: Solid  
1417 Earth*, 124, 12053–12076, 2019a.
- 1418 Pappa, F., Ebbing, J. and Ferraccioli, F.: Moho Depths of Antarctica: Comparison of Seismic, Gravity, and  
1419 Isostatic Results, *Geochemistry, Geophysics, Geosystems*, 20(3), 1629–1645, 2019b.
- 1420 Passalacqua, O., Ritz, C., Parrenin, F., Urbini, S. and Frezzotti, M.: Geothermal flux and basal melt rate in the  
1421 Dome C region inferred from radar reflectivity and heat modelling, *The Cryosphere*, 11, 2231–2246,  
1422 doi:<https://doi.org/10.5194/tc-11-2231-2017>, 2017.
- 1423 Passalacqua, O., Picard, G., Ritz, C., Leduc-Leballeur, M., Quiquet, A., Larue, F. and Macelloni, G.: Retrieval of  
1424 the Absorption Coefficient of L-Band Radiation in Antarctica From SMOS Observations, *Remote Sensing*,  
1425 10(12), 1954, 2018.
- 1426 Paterson, W. S. B.: *The physics of glaciers*, Third Edition., Elsevier, Oxford, UK., 1994.
- 1427 Pattyn, F.: Antarctic subglacial conditions inferred from a hybrid ice sheet/ice stream model, *Earth and Planetary  
1428 Science Letters*, 295(3), 451–461, 2010.
- 1429 Pfender, M. and Villinger, H.: Miniaturized data loggers for deep sea sediment temperature gradient  
1430 measurements, *Marine Geology*, 186(3–4), 557–570, 2002.
- 1431 Phaneuf, C. and Mareschal, J.-C.: Estimating concentrations of heat producing elements in the crust near the  
1432 Sudbury Neutrino Observatory, Ontario, Canada, *Tectonophysics*, 622, 135–144, 2014.
- 1433 Pittard, M. L., Galton-Fenzi, B. K., Roberts, J. L. and Watson, C. S.: Organization of ice flow by localized regions  
1434 of elevated geothermal heat flux, *Geophysical Research Letters*, 43(7), 3342–3350, 2016a.
- 1435 Pittard, M. L., Roberts, J. L., Galton-Fenzi, B. K. and Watson, C. S.: Sensitivity of the Lambert-Amery glacial  
1436 system to geothermal heat flux, *Annals of Glaciology*, 57(73), 56–68, 2016b.
- 1437 Pollack, H. N. and Chapman, D. S.: Mantle heat flow, *Earth and Planetary Science Letters*, 34(2), 174–184, 1977.
- 1438 Pollack, H. N., Hurter, S. J. and Johnson, J. R.: Heat flow from the Earth's interior: Analysis of the global data  
1439 set, *Reviews of Geophysics*, 31(3), 267–280, doi:10.1029/93RG01249, 1993.
- 1440 Pollard, D., DeConto, R. M. and Nyblade, A. A.: Sensitivity of Cenozoic Antarctic ice sheet variations to  
1441 geothermal heat flux, *Global and Planetary Change*, 49(1), 63–74, 2005.
- 1442 Pollett, A., Hasterok, D., Raimondo, T., Halpin, J. A., Hand, M., Bendall, B. and McLaren, S.: Heat flow in  
1443 southern Australia and connections with East Antarctica, *Geochemistry, Geophysics, Geosystems*, 20(11), 5352–  
1444 5370, 2019.

- 1445 Popov, Y. A., Pevzner, S. L., Pimenov, V. P. and Romushkevich, R. A.: New geothermal data from the Kola  
1446 superdeep well SG-3, *Tectonophysics*, 306(3–4), 345–366, 1999.
- 1447 Price, P. B., Nagornov, O. V., Bay, R., Chirkin, D., He, Y., Miocinovic, P., Richards, A., Woschnagg, K., Koci,  
1448 B. and Zagorodnov, V.: Temperature profile for glacial ice at the South Pole: Implications for life in a nearby  
1449 subglacial lake, *Proceedings of the National Academy of Sciences*, 99(12), 7844–7847, 2002.
- 1450 Pruss, E. F., Decker, E. R. and Smithson, S. B.: Preliminary temperature-measurements at DVDP holes 3, 4, 6,  
1451 and 8, *Antarctic Journal of the United States*, 9(4), 133–134, 1974.
- 1452 Purucker, M.: Geothermal heat flux data set based on low resolution observations collected by the CHAMP  
1453 satellite between 2000 and 2010, and produced from the MF-6 model following the technique described in Fox  
1454 Maule et al. (2005), available at: [http://webserv.cs.umd.edu/isis/images/c/c8/Antarctica\\_heat\\_flux\\_5km.nc](http://webserv.cs.umd.edu/isis/images/c/c8/Antarctica_heat_flux_5km.nc), 2012.
- 1455 Purucker, M. and Whaler, K.: Crustal magnetism, edited by M. Kono, *Treatise on Geophysics*, 5, 195–237, 2007.
- 1456 Ravat, D., Pignatelli, A., Nicolosi, I. and Chiappini, M.: A study of spectral methods of estimating the depth to  
1457 the bottom of magnetic sources from near-surface magnetic anomaly data, *Geophysical Journal International*,  
1458 169(2), 421–434, 2007.
- 1459 Rémy, F. and Legresy, B.: Subglacial hydrological networks in Antarctica and their impact on ice flow, *Annals*  
1460 *of Glaciology*, 39, 67–72, 2004.
- 1461 Rezvanbehbahani, S., Stearns, L. A., Kadivar, A., Walker, J. D. and van der Veen, C. J.: Predicting the geothermal  
1462 heat flux in Greenland: A machine learning approach, *Geophysical Research Letters*, 44(24), 12–271, 2017.
- 1463 Risk, G. F. and Hochstein, M. P.: Heat flow at arrival heights, Ross Island, Antarctica, *New Zealand Journal of*  
1464 *Geology and Geophysics*, 17(3), 629–644, 1974.
- 1465 Ritz, C.: Time dependent boundary conditions for calculation of temperature fields in ice sheets, in *The Physical*  
1466 *Basis of Ice Sheet Modelling (Proceedings of the Vancouver Symposium, August 1987)*, vol. IAHS Publ. no. 170,  
1467 pp. 207–216, Vancouver, Canada., 1987.
- 1468 Ritz, C.: Interpretation of the temperature profile measured at Vostok, East Antarctica, *Annals of glaciology*, 12,  
1469 138–144, 1989.
- 1470 Rix, J., Mulvaney, R., Hong, J. and Ashurst, D.: Development of the British Antarctic Survey Rapid Access  
1471 Isotope Drill, *Journal of Glaciology*, 65(250), 288–298, 2019.
- 1472 Rogozhina, I., Hagedoorn, J. M., Martinec, Z., Fleming, K., Soucek, O., Greve, R. and Thomas, M.: Effects of  
1473 uncertainties in the geothermal heat flux distribution on the Greenland Ice Sheet: An assessment of existing heat  
1474 flow models, *Journal of Geophysical Research: Earth Surface*, 117, F02025, doi:doi:10.1029/2011JF002098,  
1475 2012.
- 1476 Ross, H. E., Blakely, R. J. and Zoback, M. D.: Testing the use of aeromagnetic data for the determination of Curie  
1477 depth in California, *Geophysics*, 71(5), L51–L59, 2006.
- 1478 Roy, R. F., Blackwell, D. D. and Birch, F.: Heat generation of plutonic rocks and continental heat flow provinces,  
1479 *Earth and Planetary Science Letters*, 5, 1–12, 1968.
- 1480 Rudnick, R. and Fountain, D.: Nature and composition of the continental crust: a lower crustal perspective,  
1481 *Reviews of Geophysics*, (95), 267–309, 1995.
- 1482 Rudnick, R. L., McDonough, W. F. and O’Connell, R. J.: Thermal structure, thickness and composition of  
1483 continental lithosphere, *Chemical Geology*, 145(3–4), 395–411, 1998.
- 1484 Rybach, L.: Amount and significance of radioactive heat sources in sediments, *Collection colloques seminaires*,  
1485 44, 311–322, 1986.

- 1486 Salamatin, A. N., Lipenkov, V. Y., Barkov, N. I., Jouzel, J., Petit, J. R. and Raynaud, D.: Ice core age dating and  
1487 paleothermometer calibration based on isotope and temperature profiles from deep boreholes at Vostok Station  
1488 (East Antarctica), *Journal of Geophysical Research: Atmospheres*, 103(D8), 8963–8977, 1998.
- 1489 Salem, A., Green, C., Ravat, D., Singh, K. H., East, P., Fairhead, J. D., Mogren, S. and Biegert, E.: Depth to Curie  
1490 temperature across the central Red Sea from magnetic data using the de-fractal method, *Tectonophysics*, 624, 75–  
1491 86, 2014.
- 1492 Sandiford, M. and Hand, M.: Controls on the locus of intraplate deformation in central Australia, *Earth and  
1493 Planetary Science Letters*, 162(1–4), 97–110, 1998.
- 1494 Sandiford, M. and McLaren, S.: Tectonic feedback and the ordering of heat producing elements within the  
1495 continental lithosphere, *Earth and Planetary Science Letters*, 204(1), 133–150, 2002.
- 1496 Schroeder, D. M., Blankenship, D. D., Young, D. A. and Quartini, E.: Evidence for elevated and spatially variable  
1497 geothermal flux beneath the West Antarctic Ice Sheet, *Proceedings of the National Academy of Sciences*, 111(25),  
1498 9070–9072, 2014.
- 1499 Sclater, J., Jaupart, C. and Galson, D.: The heat flow through oceanic and continental crust and the heat loss of  
1500 the Earth, *Reviews of Geophysics*, 18(1), 269–311, 1980.
- 1501 Shapiro, N. M. and Ritzwoller, M. H.: Monte-Carlo inversion for a global shear-velocity model of the crust and  
1502 upper mantle, *Geophysical Journal International*, 151(1), 88–105, 2002.
- 1503 Shapiro, N. M. and Ritzwoller, M. H.: Inferring surface heat flux distributions guided by a global seismic model:  
1504 particular application to Antarctica, *Earth and Planetary Science Letters*, 223(1), 213–224, 2004.
- 1505 Shen, W., Wiens, D., Lloyd, A. and Nyblade, A.: A Geothermal heat flux map of Antarctica empirically  
1506 constrained by seismic structure, *Geophysical Research Letters*, e2020GL086955, 2020.
- 1507 Siddoway, C. S.: Tectonics of the West Antarctic Rift System: new light on the history and dynamics of distributed  
1508 intracontinental extension, *Antarctica: A Keystone in a Changing World*, 91–114, 2008.
- 1509 Siegert, M. J.: Antarctic subglacial lakes, *Earth-Science Reviews*, 50(1), 29–50, 2000.
- 1510 Siegert, M. J. and Dowdeswell, J. A.: Spatial variations in heat at the base of the Antarctic ice sheet from analysis  
1511 of the thermal regime above subglacial lakes, *Journal of Glaciology*, 42(142), 501–509, 1996.
- 1512 Slagstad, T.: Radiogenic heat production of Archaean to Permian geological provinces in Norway., *Norwegian  
1513 Journal of Geology/Norsk Geologisk Forening*, 88(3), 2008.
- 1514 Spector, A. and Grant, F. S.: Statistical models for interpreting aeromagnetic data, *Geophysics*, 35(2), 293–302,  
1515 1970.
- 1516 Stein, C. A. and Stein, S.: A model for the global variation in oceanic depth and heat flow with lithospheric age,  
1517 *Nature*, 359(6391), 123, 1992.
- 1518 Stein, C. A. and Stein, S.: Mantle plumes: heat-flow near Iceland, *Astronomy & Geophysics*, 44(1), 1–8, 2003.
- 1519 Suárez, F., Dozier, J., Selker, J. S., Hausner, M. B. and Tyler, S. W.: Heat transfer in the environment:  
1520 development and use of fiber-optic distributed temperature sensing, *INTECH Open Access Publisher Rijeka.*,  
1521 2011.
- 1522 Swanberg, C. A.: Vertical distribution of heat generation in the Idaho batholith, *Journal of Geophysical Research*,  
1523 77(14), 2508–2513, 1972.
- 1524 Talalay, P. G. and Pyne, A. R.: Geological drilling in McMurdo Dry Valleys and McMurdo Sound, Antarctica:  
1525 Historical development, *Cold Regions Science and Technology*, 141, 131–162, 2017.

- 1526 Tanaka, A., Okubo, Y. and Matsubayashi, O.: Curie point depth based on spectrum analysis of the magnetic  
1527 anomaly data in East and Southeast Asia, *Tectonophysics*, 306(3–4), 461–470, 1999.
- 1528 Taylor, S. R. and McLennan, S. M.: *The continental crust: its composition and evolution*, Blackwell Publishing,  
1529 Oxford, UK., 1985.
- 1530 Trifonova, P., Zhelev, Z., Petrova, T. and Bojadgieva, K.: Curie point depths of Bulgarian territory inferred from  
1531 geomagnetic observations and its correlation with regional thermal structure and seismicity, *Tectonophysics*,  
1532 473(3–4), 362–374, 2009.
- 1533 Turcotte, D. L. and Schubert, G.: *Geodynamics*, Cambridge University Press, Cambridge, UK., 2014.
- 1534 Ukil, A., Braendle, H. and Krippner, P.: Distributed temperature sensing: review of technology and applications,  
1535 *IEEE Sensors Journal*, 12(5), 885–892, 2011.
- 1536 Van Liefferinge, B. and Pattyn, F.: Using ice-flow models to evaluate potential sites of million year-old ice in  
1537 Antarctica, *Climate of the Past*, 9(5), 2335–2345, 2013.
- 1538 Van Liefferinge, B., Pattyn, F., Cavitte, M. G., Karlsson, N. B., Young, D. A., Sutter, J. and Eisen, O.: Promising  
1539 Oldest Ice sites in East Antarctica based on thermodynamical modelling, *The Cryosphere*, 12(8), 2773–2787,  
1540 2018.
- 1541 Veikkolainen, T. and Kukkonen, I. T.: Highly varying radiogenic heat production in Finland, Fennoscandian  
1542 Shield, *Tectonophysics*, 750, 93–116, 2019.
- 1543 Vieli, G.-M. L., Martin, C., Hindmarsh, R. C. A. and Lüthi, M. P.: Basal freeze-on generates complex ice-sheet  
1544 stratigraphy, *Nature communications*, 9(1), 1–13, 2018.
- 1545 Vitorello, I. and Pollack, H. N.: On the variation of continental heat flow with age and the thermal evolution of  
1546 continents, *Journal of Geophysical Research: Solid Earth*, 85(B2), 983–995, 1980.
- 1547 Vosteen, H.-D. and Schellschmidt, R.: Influence of temperature on thermal conductivity, thermal capacity and  
1548 thermal diffusivity for different types of rock, *Physics and Chemistry of the Earth, Parts A/B/C*, 28(9–11), 499–  
1549 509, 2003.
- 1550 van der Wal, W., Barnhoorn, A., Stocchi, P., Gradmann, S., Wu, P., Drury, M. and Vermeersen, B.: Glacial  
1551 isostatic adjustment model with composite 3-D Earth rheology for Fennoscandia, *Geophysical Journal  
1552 International*, 194(1), 61–77, 2013.
- 1553 van der Wal, W., Whitehouse, P. L. and Schrama, E. J.: Effect of GIA models with 3D composite mantle viscosity  
1554 on GRACE mass balance estimates for Antarctica, *Earth and Planetary Science Letters*, 414, 134–143, 2015.
- 1555 Wangen, M.: *Physical principles of sedimentary basin analysis*, Cambridge University Press, Cambridge, UK.,  
1556 2010.
- 1557 Wasilewski, P. J. and Mayhew, M. A.: The Moho as a magnetic boundary revisited, *Geophysical Research Letters*,  
1558 19(22), 2259–2262, 1992.
- 1559 Winsborrow, M. C., Clark, C. D. and Stokes, C. R.: What controls the location of ice streams?, *Earth-Science  
1560 Reviews*, 103(1), 45–59, 2010.
- 1561 Wright, A. and Siegert, M.: A fourth inventory of Antarctic subglacial lakes, *Antarctic Science*, 24(6), 659–664,  
1562 2012.
- 1563 Zagorodnov, V., Nagornov, O., Scambos, T. A., Muto, A., Mosley-Thompson, E., Pettit, E. C. and Tyufin, S.:  
1564 Borehole temperatures reveal details of 20th century warming at Bruce Plateau, Antarctic Peninsula, *The  
1565 Cryosphere*, 6(3), 675–686, 2012.
- 1566